NTNU

Norwegian University of
Science and Technology

STATCOM and Energy Storage in Grid Integration of Wind Farms

Sverre Skalleberg Gjerde

Master of Science in Energy and Environment
Submission date: June 2009
Supervisor: Tore Marvin Undeland, ELKRAFT

Norwegian University of Science and Technology
Department of Electrical Power Engineering

Problem Description

Offshore wind power is one of the power generation methods for the future. The floating wind farms proposed in the North Sea are promising regarding their potential for electrical power generation, but several technical challenges need to be solved. One of these is grid connection to the on-shore grid. While HVDC or HVDC-light has been proposed for transmission to the coast, the interconnections between the turbines are too short for this technology. Here AC-cables are more economical.

In an interconnection grid in a wind farm, there is a need for voltage and power stabilisation. For this purpose, a Static synchronous compensator (STATCOM) with energy storage system is proposed. The STATCOM should be able to both keep the voltage steady, and smoothen out instantaneous active power fluctuations.

In the specialisation project, the control system for the STATCOM and the energy storage was designed, and simulations to verify the system were carried out. Also, the ability to compensate active power from a wind farm was simulated. An estimate for the size of the energy storage was made.

For the master thesis, the work on the STATCOM with energy storage system should be continued, with both theoretical and practical work.

Assignment given: 27. January 2009
Supervisor: Tore Marvin Undeland, ELKRAFT

Preface

While working on this master thesis, I have learned a lot. Especially while working in the laboratory, there were quite a few things which I had to find out. Everything, from how to set up the measurments, to the implementation of the controller. This made the process of establishing the DSP controller of the lab setup quite time consuming

During the time I spent working on the realisation of the converter, some persons were very important. First of all, I have to thank visiting PhD-student, Jiri Rehacek, with whom I made the first test set up, and did the first work on the DSP. After he left, Tore Skjellnes at SmartMotor has been the most important support. Always quick to respond to questions, some of them, I have to admit, quite basic, both on set up of the lab, implementation of the control system and general problems with the SmartMotor kernel. At the final stage of the work, PhD-student Fritz Schimpf contributed with useful discussion on different matters.

In addition to these, Bård Almås and Vladimir Klubicka at Servicelaben, have been very helpful. Thank you.

During the semester, I realised that I wanted to apply for a PhD-grant. When working on this application, my supervisors, Tore Undeland and Roy Nilsen were helpful, and of great value. And there is no doubt that this has been an important motivation while working late hours in the lab, trying to overcome Murphy's law, which proved to be extremely strong there.

These 5 months of master work have been interesting, however, without my fellow students, the time spent would not have been the same. Thank you all. Especially those who have shared joys and slight despair in the laboratory together with me: Øyvind Rui, Arne Marius Ditlefsen and Hallvard Breistein. They have all contributed with moral support as well as interesting discussions. And a special thanks goes to Ragnar Ulsund, who organised the Wednesday master students' cake - an important time off during the week.

In the end I have to thank Martin Eldrup for bringing his work to the laboratory, just to sit there with me when I was doing experiments which I was not allowed to do alone.

Sverre Skalleberg Gjerde

Trondheim, June 2009

Abstract

In this work, a STAtic synchronous COMpensator (STATCOM) with energy storage system for wind power application has been treated. This device was proposed as a mean to improve voltage stability and power transmission by offering reactive as well as active power compensation. The work focuses on the converter topology of the STATCOM part and the control system. Further on, the energy storage system needed for this application was designed, including the choice of energy storage, its size and the interface/control system.

The STATCOM, reactive part of the compensator was based on a voltage source converter (VSC), using a vector control. Its purpose was to maintain a stable grid voltage.

For active compensation of wind power, a bank of super capacitors for energy storage system, SCESS, was used in this thesis. The super capacitor bank size was estimated, based upon the short term fluctuations in wind power. These fluctuations are results of contstructional factors of the turbines, variations and turbulence in the wind. The super capacitor bank was interfaced with the DC-bus of the STATCOM with a normal half-bridge buck-boost converter, to control the voltage level of the bank while maintaing a constant DC-bus voltage for good switching operation in the VSC.

The control system for the active power compensation part was implented as a cascaded PI-control, compromising an inner current control loop, and an outer power control loop. The outermost loop included a dynamical power reference, based on the actual power transfer in the grid. This reference is supposed to assure that the controller is only compensating small fluctuations, while larger changes are left for other means, for instance controlled hydro power.

The designed system was implemented in EMTDC/PSCAD. A small model, including one wind turbine, a weak grid and the STATCOM/SCESS was used in the simulations. With regards to the reactive- and active power compensation, the results were promising. However, the dynamical power reference could be of a better quality, as it does not take into account the losses in the STATCOM/SCESS, and thereby is inacurate regarding the amount power fed to/from the super capacitor bank.

In addition, a small STATCOM model was realised in the laboratory. The results from the practical work showed the same general patterns as the simulations.

Sammendrag

I arbeidet presentert her har en STAtic synchronous COMpensator (STATCOM) med energilagringssystem blitt behandlet. Denne ble foreslått som et middel for å forbedre spenningstabilitet og effektoverføring ved å kunne kompensere både reaktiv- og aktiv effekt. Arbeidet har fokusert på omformertopologi for STATCOM-delen, og reguleringssytemet. Videre ble energilagrinssystemet til denne applikasjonen designet, herunder valg av type energilager, beregning av størrelse og dets tilkobling og reguleringssystem.

STATCOM delen av kompensatoren ble basert på en spenningsmatet omformer, med bruk av vektorregulering. Hensikten med dennne reaktive delen var å opprettholde en stabil nettspenning.

For den aktive kompenseringen av vindkraften ble en superkondensatorbank (SCESS) brukt i denne oppgaven. Dennes størrelse ble beregnet basert på korte effektfluktuasjoner i vindkraft. Disse fluktuasjonene er resultatet av konstruksjonsrelaterte faktorer ved turbinene, samt variasjoner og turbulens i vinden. Superkondensatorbanken ble koblet til STATCOMens DC-bus ved hjelp av en vanlig halvbro buck-boost-omformer. Dette for å kontrollere spenningsnivået over kondensatoren samtidig som DC-busspenningen på STATCOMen ble holdt konstant for å sikre god drift av switchingen i den spenningsmatede omformeren.

Reguleringssystemet for den aktive effektkompensatoren ble implementert som en kaskade av PI-regulatorer. Den innerste reguleringsløyfen bestod av en strømregulator, mens den ytterste av en aktiv effekt regulator. Sistnevnte har en dynamisk referanse som baserer seg på den faktiske effektflyten i nettet. Den skal forsikre at det kun er mindre fluktuasjoner som glattes, mens større variasjoner i effekten overlates til andre muligheter for effektkompensering, slik som vannkraft.

Det designede systemet ble implementert i EMTDC/PSCAD for verifisering. I simuleringene ble en liten model, bestående av en vindturbin og et svakt nett i tillegg til STATCOM/SCESS-systemet. Resultatene var, med hensyn på reaktiv og aktiv effektkompensering, lovende. Men den tidligere omtalte dynamiske effektreferansen kunne hatt bedre kvalitet, siden tapene i omformerne ikke er tatt med, noe som gir en noe unøyaktig kompensering.

I tillegg til simuleringer ble en liten STATCOM-model realisert i laboratoriet. Resultatene fra dette arbeidet viste det samme generelle mønsteret som simuleringene.

Contents

List of Figures

List of Tables

List of parameters

Parameters and subscript used in the text, with explanation.

Parameter	*Explanation*
d	Real axis of Park transform
q	Imaginary axis of Park transform
o	Non-symmetric axis of Park transform
abc	Phases of 3-phase system
ref	Reference value
max	Maximum allowed value
min	Minimum allowed value
conv	Value at covnerter
p	Positive halfbridge
n	negative halfbridge
off	Offset value

Table 1: Subscript used in the text

Parameter	*Explanation*
f_s	Synchronous frequency
ω_s	Synchronous pulsation, equals $2\pi f_s$
ω_r	Mechanical, rotational speed of the wind turbine
L	Inductance
V_2	Voltage, AC-side of VSI
V_1	Voltage, at PCC
i	AC-side current of STATCOM
V_{dc}	DC-bus voltage
I_l	DC-bus current
C	DC-bus capacitor
R	AC-side resistance of STATCOM
θ	Angular position of supply voltage vector
V_r	Reference voltage signal for PWM-generation
ζ_s^s	Voltage space vector angle
t	Switching period
V	D,q-transformed AC-voltage
T_n	Regulator parameter
T_i	Regulator parameter
T_{pE}	Small time constant
T_e	Sample time
T_{cm}	Time constant of the inverter
T_{mes}	Time constant of measurement delay
T_r	Signal processing delay
I_{dc}	Current at DC-bus
T_e	Sample time
f_{sw}	Switching frequency
S_n	Nominal power
i_{rp}	Current ripple
L_2	Grid side inductance of filter
L_1	STATCOM side inductance of filter
C_f	Shunt filter capacitor
f_{res}	Filter resonance frequency
V_n	Nominal voltage
I_n	Nominal current
f_n	Nominal frequency
T_{df}	Time constant of filter for active damping
C_{scap}	Super capacitor
W_{scap}	Super capacitor energy

Table 2: Parameters used in the text

Abbreviations

In the following table, abbreviations used in the text are explained.

Abbreviation	*Explanation*
VSI	Voltage source inverter
CSC	Current source converter
STATCOM	STATic synchronous COMpensator
PWM	Pulse width modulation
PCC	Point of common coupling
VOC	Voltage oriented control
SVC	Static var compensator
SVPWM	Space vector pulse width modulation
ESS	Energy storage system
BESS	Battery energy storage system
SCESS	super capacitor energy storage system
SCAP	Super Capacitor
PLL	Phase locked loop
L-filter	Electrical filter, compromsing only an inductance
LCL-filter	Electrical filter consisting of two inductances with capacitor in shunt
NPC	Neutral-Point Clamped

Table 3: Abbreviation used in the text

1 Introduction

In both the world of science and politics, most people agree upon the fact that there is a global warming issue, and that it is created by human activities. A lot of initiatives have been taken throughout the world to limit the emitions of green house gases, especially within the energy sector. In the European Union, are 80 % of the green house gases emitions related to energy production [1]. The EU has agreed upon their by now well known 2020 goals for reduction of green house gases emissions and energy use [2].

To achieve these goals, technologies for new renewable energy must be developped. Since energy is one of the key factors for a wealthy society, the technologies which offers an alternative to oil, gas and coal will be important for the future. Among all the emerging renewable energy sources, like solar-, tidal-, wave- and wind power, the latter shows the greatest potential in a short term perspective. In addition, wind power offers the most mature technology. However, moving towards larger wind farms, and especially those planned offshore in Great Britain, Germany, Denmark and Norway, will rise the wind power penetration in the grid to a level where it will have a major impact to the operation of the power system. In such a situation, the nature of the wind power, with small units, and fluctuations in the power can be a source of problems, and in a worst case scenario, jeopardise the stability of the power system.

To avoid such a situation, several measures have been proposed. For long term balancing of wind power, the Norwegian hydro power system is well suited, with fast power regulation capability compared to that of thermal power. However, when considering the short term fluctuations due to e.q. turbulences, are these to fast to be compensated by the hydro power. Hence another mean for doing so is desirable.

Considering this demand for active power regulation, and the fact that normally reactive power compensation is needed in connection with a wind farm, a STAtic synchronous COMpensator (STATCOM) with energy storage system (ESS) is proposed. The purpose of this is to include both active- and reactive compensation in the same device.

In this work, the STATCOM/ESS will be treated. The main focus will be on the converter topology for the STATCOM and its control system. This will both be treated theoretically, in simulations, and through practical implementation in laboratory. In addition, the energy storage system will be treated theoretically and simulated.

For practical verification of the simulations, a laboratory experiment was established. An excisting converter was modified and a DSP controller was implemented.

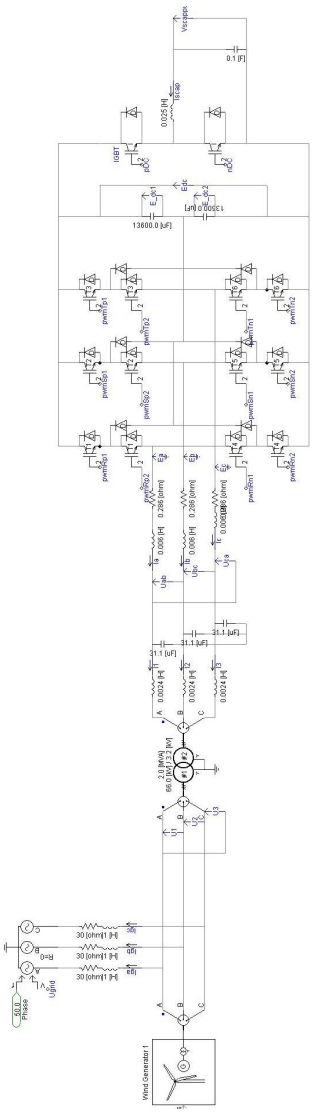

Figure 1.0.1: The power system simulation model used in the work

2 Background and Theory

2.1 STATCOM

A STATCOM (Static synchronous Compensator) is a shunt, flexible AC transmission system (FACTS) device, used to compensate the reactive power in a grid, and by this stabilise the grid voltage. A stable grid voltage will also improve the power transmission of the system, since the transfer of power is depending on the system voltage. In addition, the FACTS can be used to improve the stability of the interconnection between two AC-systems. [20].

The STATCOM is, in contradiction to the more traditional Static Var Compensator (SVC), not depending on the applied voltage for injecting or absorbing the demanded reactive power. This ability makes the STATCOM advantageous for regulation of the system voltage at the point of common coupling (PCC).

There are two variants of STATCOM, the current-source converter based (CSC) and the voltage source converter (VSC)/voltage source inverter (VSI) based. In this work only the latter will be treated.

The VSC-based STATCOM compromises a Pulse Width Modulation (PWM)-controlled 3-phase inverter with a DC-bus capacitor. In contradiction to the traditional reactive compensators, such as condenser banks, where the capacitor size is directly related to the compensating capability, the DC-capacitors of the STATCOM are of no direct connection to the reactive power supply. Its only purpose is to maintain a steady DC-bus voltage. A simplified circuit scheme of a VSC STATCOM is given in fig. 2.1.1. For more information on the basic operation of the VSC, see [20].

The 3-phase voltage of the system can be expressed as following (eq. 2.1.1), if considering an AC-side single-inductance filter (L-filter), according to [19].

$$v_{2,abc} = Ri_{abc} + L\frac{di_{abc}}{dt} + v_{1,abc} \tag{2.1.1}$$

Applying the Clark- and Park transforms,presented in [24], to eq. 2.1.1, yields the following set of equations, eq. 2.1.2 and eq. 2.1.3, describing the converter in the d,q-reference frame:

$$v_{1d} = Ri_d + L\frac{di_d}{dt} - \omega Li_q + v_{2d} \tag{2.1.2}$$

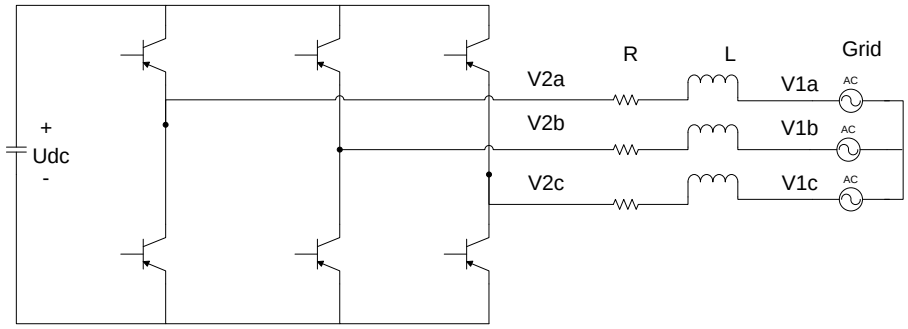

Figure 2.1.1: The VSC STATCOM circuit scheme

$$v_{1q} = Ri_q + L\frac{di_q}{dt} + \omega Li_d + v_{2q} \tag{2.1.3}$$

The current/voltage relation across the capacitor is:

$$C\frac{dV_{dc}}{dt} = I_l \tag{2.1.4}$$

2.2 Multilevel converter

The use of a 2-level converter implies a simple control system for the VSI with no need of DC-bus balancing, and a simple switching scheme. But the system itself has several drawbacks. First, the IGBTs have to hold the whole DC-bus voltage, which in megawatt-rated converters is several kilovolts. In addition, the losses in the device are higher, and the switching generates higher harmonics, [17]. This will demand for higher filtering capacity. Hence, the use of a multilevel converter is preferable.

In [17] several multilevel converters are presented. For this work, the 3-level, Neutral-Point Clamped (NPC) converter was chosen. The complexity of this is not far from that of the 2-level VSI, but the improvements in performance are significant. This converter type is available with medium voltage and MW-rating today.

The main difference between the operation of the 2-level and the 3-level converter is the PWM-generation. While the 2-level generator compromises one triangular carrier pulse varying between -1 and 1, the 3-level compromises two signals, one between -1 and 0, and one between 0 and 1. The carrier

signals have the same frequency and phase, or the phase could be shifted 180^o.

The additional switches allow the system to operate at 27 different states, compared to the 8 of the 2-level. This yields a better switching pattern and -characteristics, as each switching operation only will switch with a step of $\frac{V_{dc}}{2}$. The different levels are shown in fig. 2.2.1, in a space vector representation.

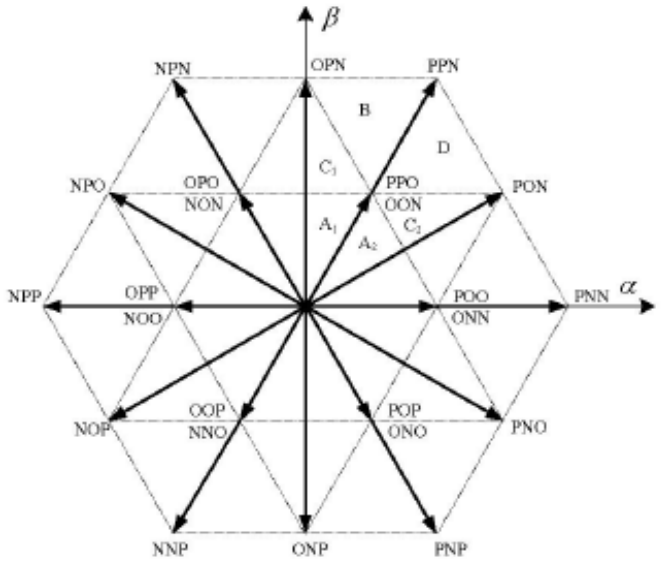

Figure 2.2.1: Possible outputs from a three-level converter

2.3 PWM-modulation

The PWM-strategies for switching the inverters are the most common ways of controlling the transistor based converter. These strategies offer a low harmonic content in the output of the inverter compared to square wave modulation (SWM). This is related to the on/off time of the switches. While the latter method has a constant switching period, the PWM technique yields a changing switching time, depending on the demanded output voltage. There are several different PWM-techniques which all have their advantages and disadvantages. These are treated in [11]. The one applied here is normally referred to as sinusoidal PWM-modulation with 3^{rd}-harmonic injection, or carrier based PWM (CBPWM). A summary of the technique is given below.

2.3.1 Sinusoidal PWM with 3^{rd} harmonic injection

This method introduces a 3^{rd} harmonic to the phase voltage, while the line-voltage is the same, because the same 3^{rd} harmonic is injected to all three phases.

The output signal can be described by the following

$$V_a = V_r(\cos(\zeta_s^s + M_3(3\zeta_s^s)) \tag{2.3.1}$$

$$V_b = V_r(\cos((\zeta_s^s - 120^0) + M_3(3\zeta_s^s)) \tag{2.3.2}$$

$$V_c = V_r(\cos((\zeta_s^s + 120^0) + M_3(3\zeta_s^s)) \tag{2.3.3}$$

Where ζ_s^s is the rotational angle of the sinusoidal system and M_3 is the amplitude of the injected 3^{rd}-harmonic.

This swithcing scheme yields a maximum sinusoidal range of $\frac{2}{\sqrt{3}}$ pu.

It is possible to obtain higher voltage with over-modulation, but this would cause a non-sinusoidal output voltage, which results in a higher harmonic content, and thus aditional filter capacity is required.

2.3.2 Switching pattern for 3-level converter

The switching patterns for one branch in the 3-level converter are shown in fig. 2.3.1. Applying a positive voltage of $\frac{V_{dc}}{2}$ correspond to turninng on the two uppermost IGBTs. -$\frac{V_{dc}}{2}$ corresponds to the two down most switches

being turned on. Neutral voltage is applied by using the two IGBTs in the middle of the branch. The smaller voltage steps in the switching operations are favorable with regards to the harmonics injected in the grid.

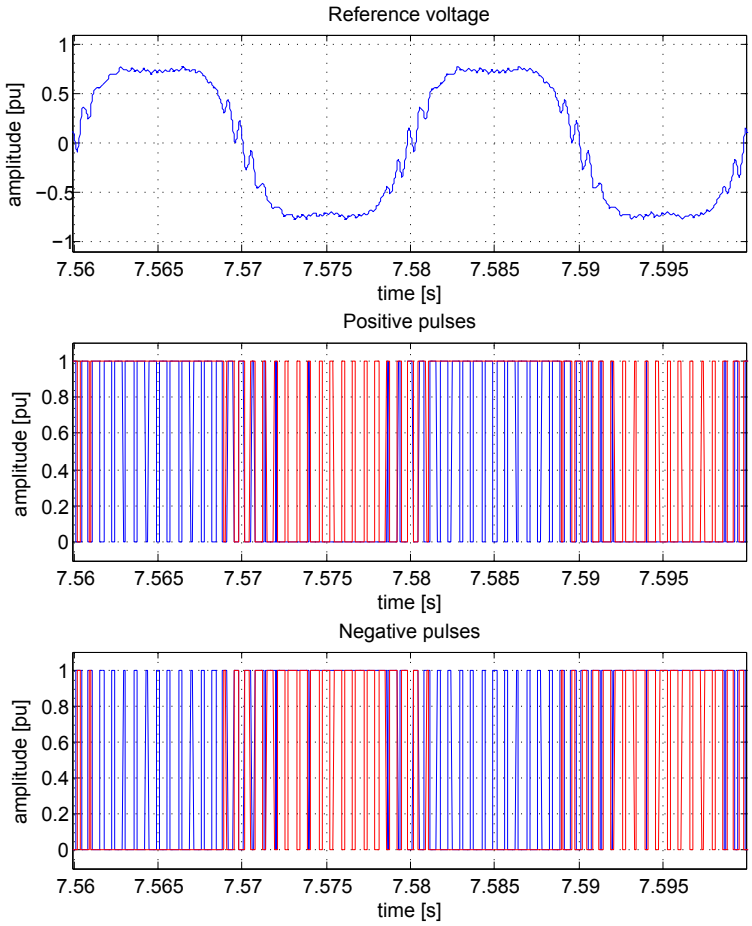

Figure 2.3.1: The switching patterns and the corresponding reference voltage.

The inputs to the PWM-generator, for one branch, with the carrier signals, are shown in fig. 2.3.2.

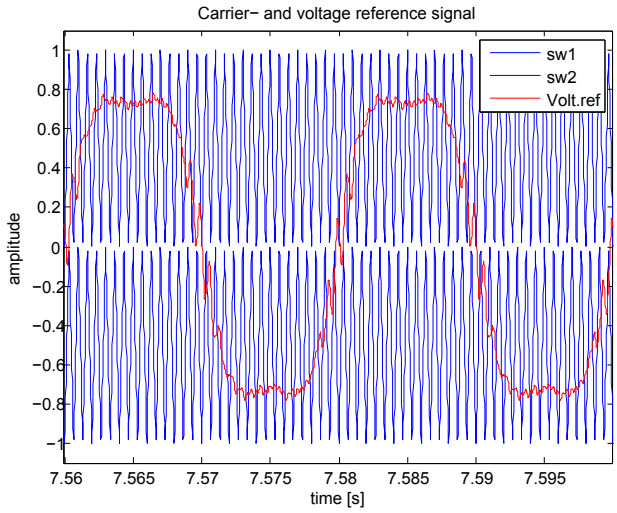

Figure 2.3.2: PWM-generator reference signals

The two carrier signals have a pulse of 1.5 kHz, and the plot is taken from the steady state of a three-level inverter simulated, hence the time axis. The switching pulses are generated by comparison of the carrier and the reference signal, and the possible outputs of one branch are listed in tab. 2.3.1. In fig. 2.3.1, the resulting switch patterns are given, together with the reference signal. "Positive pulses" is referring to the two uppermost transistors, while "Negative pulses"' refers to the two down most.

Transistor	$V_{ref} > V_{tri,up}$	$V_{ref} < V_{tri,up}$	$V_{ref} > V_{tri,down}$	$V_{ref} < V_{tri,down}$
T_{p1}	1	0	0	0
T_{p2}	1	1	1	0
T_{n1}	0	1	1	1
T_{n2}	0	0	0	1

Table 2.3.1: Switching states of the inverter, one branch, as function of reference- and carrier signals

2.3.3 Balancing of the DC-bus voltages

The use of multilevel NPC-converter demands for active balancing of the DC-bus voltage. This is because there are two separate capacitor banks, which should have the DC-voltage equally shared to assure an equal switch operation. Unequal loading could change this. Therefore, several techniques have been developed to maintain the two capacitor voltages at the same level. The one applied in this work is presented in [15]. It is based on modifying the voltage references, which are fed to the PWM-generator. Here presented for phase A in eq.2.3.4.

$$v'_a = v_a - v_o \tag{2.3.4}$$

Where v_o is given by eq. 2.3.5.

$$v_o = \frac{max(v_a, v_b, v_c) + min(v_a, v_b, v_c)}{2} \tag{2.3.5}$$

The modified signal is divided in two parts. One for the positive carrier, subscripted "p", and one for the negative, subscripted "n".

$$v'_a = v_{ap} + v_{an} \tag{2.3.6}$$

The optimal solution for the voltage balancing is given in eq. 2.3.7

$$v_{ap} = \frac{v_a - min(v_a, v_b, v_c)}{2} v_{an} = \frac{v_a - max(v_a, v_b, v_c)}{2} \tag{2.3.7}$$

For compensating eventual offsets, which would make the eq. 2.3.6 invalid, the offset is calculated from eq. 2.3.8, and subtracted from the input signals to the PWM-generator.

$$v_{ioff} = k_p |\Delta v_c| sign(\Delta v_c i_i) sign(v_{ip} - v_{in} - 1) \tag{2.3.8}$$

Where Δv_c is the difference in voltage between the two capacitors of the DC-bus.

2.4 STATCOM control system

The full control system of the STATCOM/SCESS is presented in fig. 2.4.1. The details are treated in the following sections.

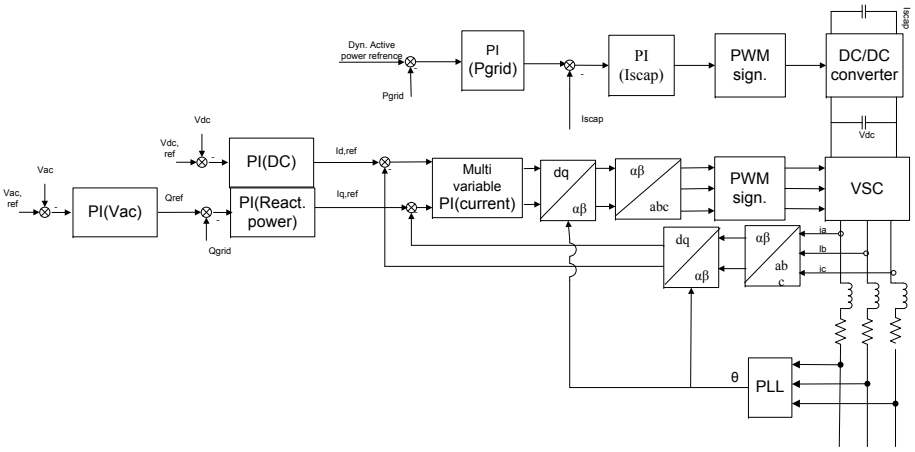

Figure 2.4.1: The full control system of the STATCOM/SCESS

2.4.1 Vector control for the VSC

While the amplitude of the control variable is the only variable controlled in classical control of an electrical system, vector control offers the possibility to control both the magnitude and the phase of the variable. This yields, according to [6] better dynamical response in the system.

The vector control is based on imposing and controlling the real and imaginary part of the controlled variable.

When applying the vector control to a 3-phase system, there is a linkage between the d- and q- axis caused by inductive or capacitive elements, as seen from eq. 2.1.2 and eq. 2.1.3. This is cross-coupling between the axis' is taken into consideration by adding a feed forward term to the controller.

To minimise the influence of this coupling, a multivariable is applied, allowing the system to be fully decoupled in the d- and q-axis. The modeling presented here compromises an inductive filter for the AC-circuit, while for the full system, a LCL-filter will be used. The resonance problems this filter might cause are controlled by adding damping to the control system, see sec. 2.6.

Hence, the current controller can be constructed as there is only the inductive AC-filter.

The following is based on the assumption that the switching frequency of the converter is high enough for assuming that the transfer function of the inverter being completely real. The requirements for doing so is treated in [6].

Transfering the linear, complex equations eq. 2.1.2 and eq. 2.1.3 to a transfer function yields

$$\frac{\underline{i}(s)}{\underline{v}(s)} = \frac{\frac{1}{R}}{(1 + (s + j\omega)L/R)} \tag{2.4.1}$$

To decouple the system, the following controller is introduced, which compensates the dominant, complex pole of the system.

$$\underline{G}_r = \frac{(1 + (s + j\omega)T_n)}{sT_i} \tag{2.4.2}$$

Where the regulator parameters T_n and T_i are chosen as follows, according to the modulus optimum criterion, [5].

T_n=T_t=R/L
T_i=2KT_{pe}=2V_e/R(T_e/2+T_{cm}+ T_{mes}+T_r)

Where T_{pe} is the estimated small time constant, and the different time constants are defined as following:

T_e = Sample time
T_{cm} = Time constant of the inverter (i.e., the time delay introduced by the switching frequency). This is estimated as $1/(f_{pulsation} \cdot 3)$.
T_{mes}= Time constant introduced by the measurements delay.
T_r = Time delay introduced by the signal processing (only used in implementation of the physical system).

The block diagram for the multivariable PI-regulator is represented in fig. 2.4.2. The transfer function block represents the PI-regulator, while the $\mathrm{l} \cdot w_s$ feed forward branches of the currents are the imaginary parts of the complex transfer function in eq. 2.4.2. These feed forward terms are compensating the cross-coupled inductive terms of eq. 2.1.2 and 2.1.2.

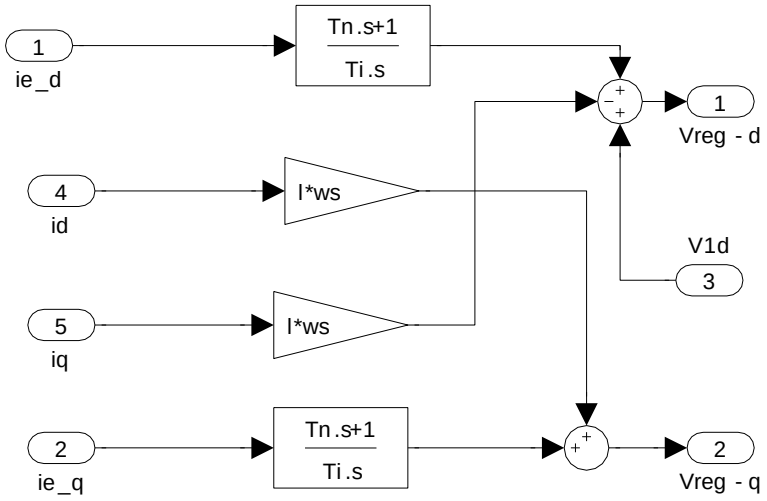

Figure 2.4.2: Block diagram, multivariable PI-regulator

2.4.2 Secondary control loop

The secondary control loop for the STATCOM is controlling the voltage of the DC-bus capacitor, and the reactive power exchanged with the grid. The outputs of these controllers serves as references for the current controllers.

The relation between the DC-bus and the converter output voltage is, in steady state, per unit:

$$v_{dc}i_{dc} = v_d i_d \tag{2.4.3}$$

And the reactive power is in steady state:

$$q = v_d \cdot i_q \tag{2.4.4}$$

If the voltage is assumed to be constant, current controller can take the output from the DC-voltage control (d-axis) and reactive power control (q-axis) output as references.

T

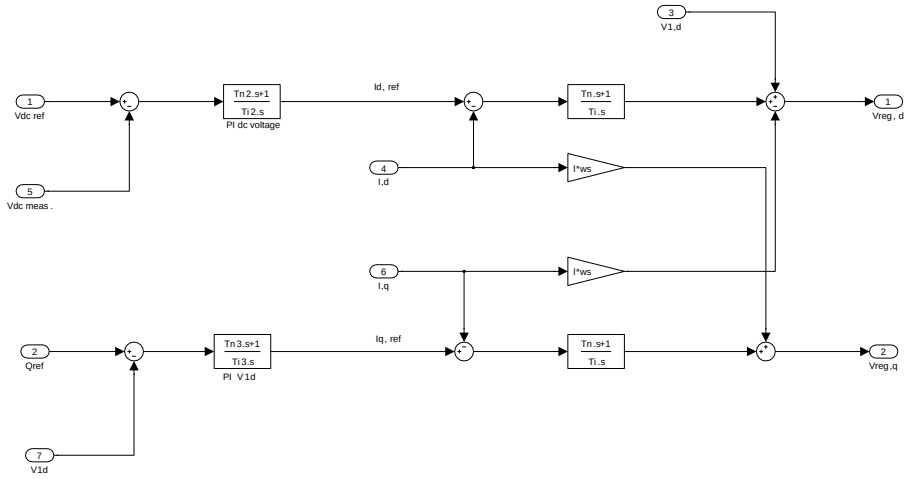

Figure 2.4.3: Block diagram, current and voltage controllers

The design of parameters for this control is performed with the symmetrical criterion, which is to be found in [5]. A summary of the equations used to calculate the parameters is given in eq. 2.4.5 and 2.4.6.

$$T_n = 4T_{pE} \tag{2.4.5}$$

$$T_i = \frac{8(T_{pE})^2}{Ti} K_{cm} = \frac{8(T_{pE})^2}{C} \tag{2.4.6}$$

Where $T_{pE} = 2T_{cm}$.

2.5 LCL-filter

In the sections above, an inductor AC-filter has been used for the sake of simplicity. However, introducing the slightly more complex LCL-filter (two inductances in series, with a capacitor in shunt) at the AC-side of the converter will help to improve the damping of switching harmonics injected in the grid, and the size of the inductor can be reduced, according to [13]. The design method of the LCL-filter carried out in this work was treated in [26].

The design is based on the following steps:

First finding the total filter inductance

$$L = \frac{V_{dc}}{8 i_{rp,max} f_{sw}} \tag{2.5.1}$$

Where $i_{rp,max}$ is the maximal allowed ripple and f_{sw} is the switching frequency of the converter.

Then, defining the ratio between the inductance and the capacitor:

$$x = \frac{3\omega_n V_2^2}{\omega_{sw} L S_n \lambda} \tag{2.5.2}$$

Where λ is defining the ratio of reactive power absorbed by C_f, ω_{sw} is the angular switching frequency, $omega_n$ is the angular frequency of the grid and L is the total inductance.

Finally, the following relations can be applied:

$$L_2 = \frac{1}{a+1} L \tag{2.5.3}$$

$$L_1 = a L_2 \tag{2.5.4}$$

$$C_f = \frac{1}{r \omega_n^2 L_2} \tag{2.5.5}$$

The resonance frequency is given by eq. 2.5.6:

$$f_{res} = \frac{1}{2\pi} \sqrt{\frac{L_1 + L_2}{L_1 L_2 C_f}} \tag{2.5.6}$$

2.6 Active damping

The use of a LCL-filter to filter out harmonics introduced by the STATCOM requires damping. This is due to the resonance frequency of the filter, which might cause instability in the system. There are different ways of doing this. One option is to introduce an additional resistor to the filter, but this will cause higher losses in the system. Another way of damping the oscillations is by introducing an active damping to the current controllers [25]. The main purpose of the active damping is to reduce the system's frequency response

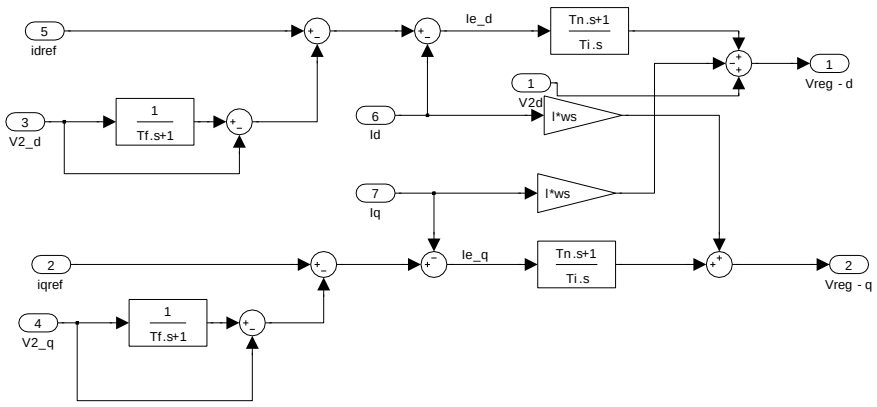

Figure 2.6.1: The current control with active damping

The active damping takes the d,q-transformed voltages as input. It is filtered and subtracted from the original signal, leaving only the ripples left. The resulting signal is fed to the current reference of the PI-controller. In order to make the active damping efficient, the bandwidth of the filter should be small enough to filter out the resonance frequency of the LCL-filter.

2.7 Anti-windup for PI-controller

When using a pure PI-controller, the physical limit of the system could be reached. If this situation occurs while there is still a deviation between the reference and the output of the system, the integrator term of the controller saturates. This leads to a the system acting as open loop transfer function, and hence, the system could become instable. To avoid this problem, different anti-windup strategies have been developed. The one which is chosen here is presented in [7], and is referred to as back-calculation.

The principle is to add a term to the integral input, which is active when the regulator output exceeds the saturation limit of the system. This yields the following input to the integrator, eq. 2.7.1

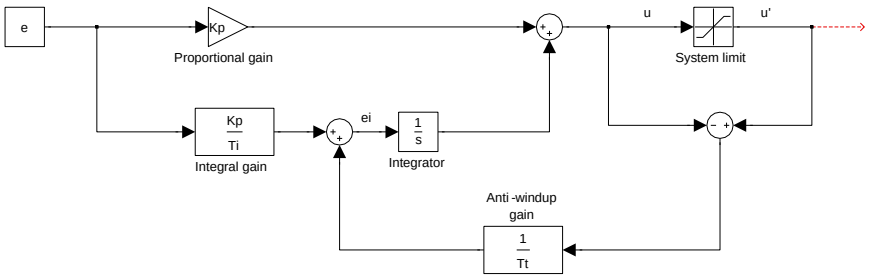

Figure 2.7.1: PI-controller with anti-wind up

By applying such a controller, the overshoot in the transients of the system is be better controlled than without. In addition, the stability margin is improved, as there are no time delays introduced by the discharging of the integrators.

2.8 Droop control for the PCC-voltage control

The ability to control the voltage is limited by the VA-rating of the STATCOM/SCESS system. The relation between voltage drop and reactive power

is given in eq. 2.8.1, from [12].

$$\Delta V_x = \frac{\omega L_{line}}{V_x} \Delta Q \tag{2.8.1}$$

As seen, this can depending on the line inductance easily lead to saturations in the controllers if the voltage deviates significantly from the nominal voltage. In these cases a droop control is advantageous. This is realised by modifying the voltage reference so that the reactive power demand never exceeds the limit of the system, i.e. Q_{ref}=1.0 pu. When Q_{ref} is within the system limits, the voltage reference is kept at 1.0 pu, but when the reactive power demand rises above this threshold, the voltage reference is descending linearly. Hence, the nature of the droop control is quite similar to that of the anti-windup, but affecting the reference instead of the integral term. The droop applied to the voltage reference is given in eq. 2.8.2

$$\begin{cases} \Delta V = 0 & \text{if} Q_{inj} < 1.0 \\ \Delta V = K_{droop} Q' & \text{if} Q_{inj} \geq 1.0 \end{cases} \tag{2.8.2}$$

Where K_{droop} is a constant between 0 and 1, and Q' is the amount of reactive power which would have been injected if there was no droop control to the reference. A simple droop control for the simulations is presented below, in fig. 2.8.1

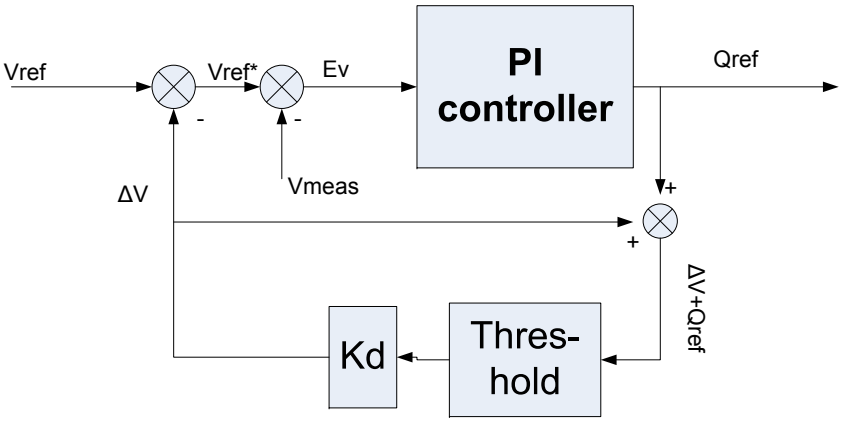

Figure 2.8.1: DC/DC-converter for super capacitor bank

2.9 STATCOM rated values

The system ratings used in this work are based on present, industrial common values. A nominal line voltage of 3.3 kV for a 3-level NPC inverter is common for megawatt motor drives. The drives have close to the same structure as a VSI-based STATCOM, and therefore, this value is used for the design of the STATCOM/SCESS.

The MVA-ratings of the STATCOM decides the switching frequency, which is normally limited by thermal restraints to the device, and thus also the current. But, a low switching frequency causes undesired cross-coupling effects in the current control, and low order harmonics with large amplitude. Hence, the switching frequency is kept as high as possible. According to [20], the frequency modulation, defined in eq. 2.9.1, should be kept ≥ 21 for an asynchronous PWM-scheme, as that implemented here. With a fundamental frequency of 50 Hz, this implies a minimum f_{sw} of 1050 Hz. Considering the constraints mentioned here, a frequency of 1500 Hz is used for the inverter switching of the VSCs.

$$m_f = \frac{f_{sw}}{f} \tag{2.9.1}$$

The dimensioning of the STATCOM with regards to the reactive power capability depends on the size of the wind farm, the choice of generator- and eventual converter technology in the turbines, and the transmission lines to the PCC. In addition, a hybrid reactive compensation system is normally chosen, combining STATCOM and capacitor banks. Evaluating this is not of any interest for this work which is focusing on the control of a STATCOM/SCESS and the converter structures. Hence, only a reasonable value is chosen. The type of converter, and the switching frequency implies a rating of up to about 10 MVA. However, to keep the size of the simulation files, and hence also the simulation time, down, the rating of the STATCOM is set to 2 MVA.

2.10 Energy storage system

2.10.1 Generalities

In wind farms, not only the reactive-, but also the active power is fluctuating. These fluctuations should be controlled, in order to obtain a more sta-

ble power system, both with regards to the power transmission and voltage. For this purpose, the STATCOM with an energy storage system (Normally named STATCOM/ESS) has been proposed in [3]. Several different techniques for storing energy are available, each having their advantages and disadvantages regarding lifetime, power density and energy density: Batteries, fly-wheels, super capacitors and super conducting inductors. The literature considers normally battery energy storage systems, while some newer [8], [27] also take into consideration the super capacitors.

Due to the power fluctuations in a wind farm, there is a need for high power for a short period in order to maintain a stable voltage. For this purpose, the super capacitor is the most suitable choice, offering high power density, while the energy density is low, compared to for instance batteries. Since the purpose of the device is not to store energy, but smoothen out the active power fluctuations, this is an acceptable trade-off. In addition, the high number of cycles the super capacitors can handle are also favourable.

By adding the energy storage element, the STATCOM can draw and inject both active and reactive power, adding an additional degree of freedom to the system. By doing so, the power quality is improved. The demanded size of the energy storage system is depending on the demanded control of the power fluctuations. A sensitive control will demand for a higher energy capacity than a rough one.

In fig. 2.10.1 the principle of the system is shown, here presented with a 2-level converter.

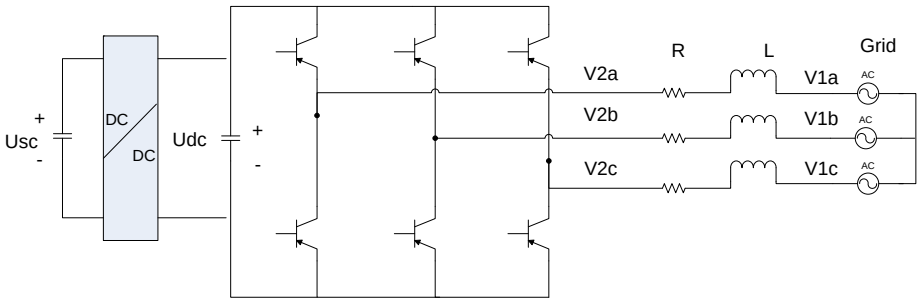

Figure 2.10.1: The STATCOM with super capacitor

2.11 Control strategy for energy storage system

There are several proposed ways of controlling a STATCOM/SCESS in the literature for instance in [21]. However, these seem rigid and heavy. Therefore, a new strategy, proposed by [23], is investigated.

2.11.1 Proposed control principle

The control principle investigated here compromises a system with disconnected STATCOM and DC/DC-converter control. This in order to omit the change of reference for the STATCOM-controller. The power controller is needed to be slower than the DC-bus controller, so the latter voltage can be kept steady. Also, there is a need to introduce an upper- and lower voltage limit for the super capacitor to avoid instabilities in the DC/DC-converter.

To ensure that only small ripples in the active power are filtered out, as the system will not be dimensioned for compensating major changes in power output from the wind farm, the reference for the active power controller should be dynamic. This is solved by controlling the deviation between the actual power and the reference. If the deviation of the latter is to large compared to the system's dimensions, the reference is changed a small step, ΔP. The same is done if the super capacitor bank becomes fully discharged/charged, since the system will not be able to compensate fluctuations during such conditions.

2.12 DC/DC-converter for super capacitor

The super capacitor bank needs an interface for the connection to the DC-bus. This could span from a simple inductance to filter out the most severe ripples, to a full bridge DC/DC-converter. The choice depends very much on the demanded size of the energy storage, as the cost (and size) of the converter should be compared to that of the super capacitors.

The general system, seen from the super capacitor bank is presented in fig. 2.12.1. The variable load will in the case treated in this text be the grid interfaced with the VSC of the STATCOM.

[1]

[1] Fig. 2.12.1 is taken from [10]

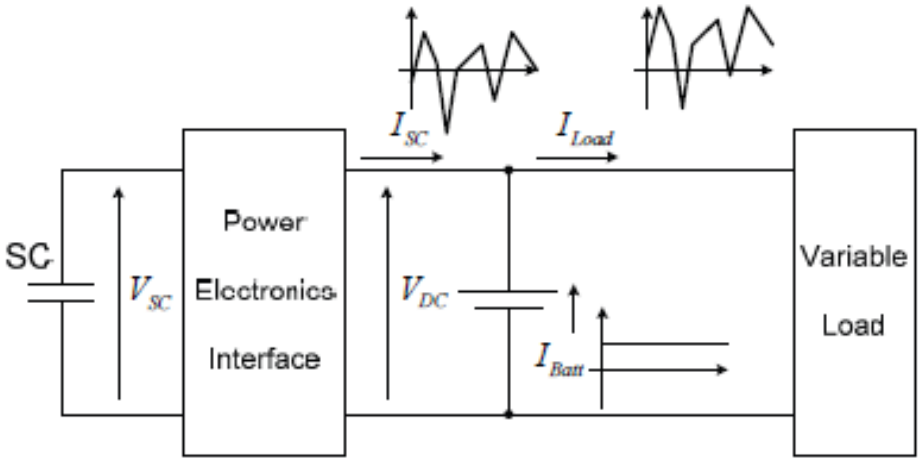

Figure 2.12.1: General super capacitor system

In [4] a half-bridge buck-boost converter is presented. This compromises two bidirectional switches, an inductor and the super capacitor bank. The converter is depicted in fig. 2.12.2. The converter command is a carrier based PWM signal, fed from a cascaded controller. The innermost controls the current, while the outermost feeds this controller based on the active power correction needed in the PCC.

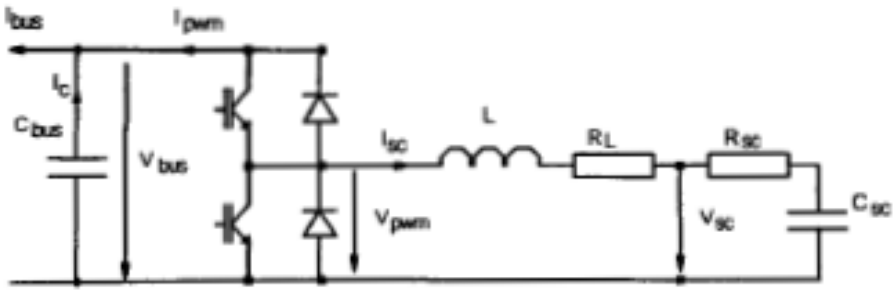

Figure 2.12.2: Half-bridgde buck-boost converter.

[2]

2.12.1 Current control for the DC/DC-converter

In [18], a current controller for a DC/DC-converter super capacitor application is given. A short summary of this is given below.

[2]Fig. 2.12.2 is taken from [4]

The current control loop, with the super capacitor can be expressed as, eq. 2.12.1

$$F_{bf} = \frac{K_{psc}s + K_{isc}}{L_{dc,filt}s^2 + K_{psc}s + K_{isc}} \tag{2.12.1}$$

This yields the following expressions for the controller parameters, K_{psc} and K_{isc}:

$$K_{psc} = 2\epsilon L_{dc,filt}\omega_n \tag{2.12.2}$$

$$K_{isc} = L_{dc,filt}\omega_n^2 \tag{2.12.3}$$

Where ω_n=$2\pi f_{sw}/10$, and the damping ϵ=0.707. The DC-filter inductance $L_{dc,filt}$ is calculated as follows from eq. 2.12.4:

$$L_{dc,filt} = \frac{U_{s,cap}}{8 f_{sw} \Delta I_L} \tag{2.12.4}$$

2.13 On the nature of the active power fluctuations in a wind farm

The active power control of the STATCOM/SCESS system is required to follow the mean power production of the wind farm. For estimation of the time response of this controller, and its dynamical reference system, the fluctuations in the power output from a wind farm should be take into consideration. These fluctuations can, according to [9] be expressed as:

$$P_m = P_{mo} + \Delta P_m \sin \omega_1 t \tag{2.13.1}$$

Where P_m is the mechanical, instantaneous power, P_{mo} is the mean mechanical power, and ω_1 is fluctuations corresponding to the fluctuations in the wind.

In addition, there is a constructional factor; the shadowing effect of the tower each time a blade passes it. This will cause a pulsating torque, and hence power, with a frequency of $3{\cdot}\omega_r$.

[9] shows that these mechanical power fluctuations could cause fluctuating power and current, and therefore, an active power filtering of these is desirable. Hence, the reference and feed back loop of the active power control should be designed so that these are eliminated.

2.14 Discrete control system

For digital implementation, the control system, which for the simulations was kept in a continuous state, should be discretized. When passing from continuous to discrete system, the approximation presented in [14] was used. This approximation, used for estimating the discrete values, is a first order trapezoidal integration. The following relation between the continuous and sampled state, 2.14.1, is applied here.

$$s = \frac{2}{T_{st}} \frac{1 - z^{-1}}{1 + z^{-1}} \tag{2.14.1}$$

Where, T_{st} is the sample time used in the system, and z^{-i} refers to the time step. i=0 equals present time, while i=1 equals the last step.

When discretising a system, the main rule for choice of sampling time is $T_{sample}<T_{pe}/2$. This is referred to as "'théoreme de l'échantilonnage"', or the sampling theorem in [16]. If the theorem is respected, the original signal can be reconstructed perfectly from the sampled.

3 Synthesis of the control system

3.1 The continuous control system

3.1.1 General

The control system, with the chosen control strategy, and the system build up is presented in sec. 2.4. In this section, the resulting control parameter values are presented, based upon the system implemented in the simulations.

3.1.2 LCL-filter design

Since the STATCOM side inductance of the LCL-filter is determing the parameters of the current controllers, the design of this filter should be carried out first. The input parameters of the design were the STATCOM parameters (tab. 3.1.1) and the ones specific for the filter (tab. 3.1.2).

Parameter	*Value*
S_n	2.0 MVA
V_n (RMS)	3.3 kV
I_n	350 A
f_n	50 Hz
V_{dc}	6 kV
f_{sw}	1.5 kHz

Table 3.1.1: System parameters

See sec. 2.9 for discussion on the system ratings.

Parameter	*Value*
$I_{rp,max}$	12 %
λ	0.05

Table 3.1.2: Filter constraints

The resulting filter parameters are listed in 3.1.3

Parameter	*Value*
L_1	6.0 mH
L_2	2.4 mH
C_f	31.1 μF

Table 3.1.3: System parameters

3.1.3 Current controller

The current controller was designed applying the optus modulus criterion, treated in sec. 2.4, where the switching frequency was introduced as time delay. Only the L_1 part of the filter was considered, as the active damping is assumed to damp out the response of the LC-part.
The resulting open loop transfer function for the reference, i_{ref}, is

$$\frac{\underline{i}}{\underline{i}_{ref}} = G_o = \frac{1/R}{sT_i(1+sT_{cm})} \tag{3.1.1}$$

As seen, the coupling has been eliminated, making the control of current decoupled in a d, and q-axis. (Like treated in [6], this is only valid for relatively high frequency switching.)

The parameters used in the synthesis and in the later simulations are listed below, in tab. 3.1.4, and in tab. 3.1.1.

Parameter	*Symbol*	*Value [pu]*
Filter resistance	R	0.286 Ω
Filter inductance	L_1	6.0 mH
DC-bus capacitor	C	6800 μF

Table 3.1.4: Electrical parameters for regulator design

[3]

Applying the above listed parameters to the control theory yields the following parameters for the current controllers.

[3]DC-bus capacitor value from [11]

Parameter	*Value*
T_n	0.0209
T_i	0.0104

Table 3.1.5: Current controller parameters

3.1.4 Outer controllers

The outer control loop is described in sec. 2.4.2. The time constants of the closed current loops are the design parameters used for the final design. The closed loop transfer function, as a first order approximation, is given in eq. 3.1.2:

$$\frac{\underline{i}}{\underline{i}_{ref}} = \frac{1}{1 + s2T_{cm}} \tag{3.1.2}$$

3.1.5 DC-bus controller

The DC-bus voltage control was designed by applying the symmetrical criterion, treated in 2.4.2. The DC-link capacitor value and the T_{cm} from eq. 3.1.2 are design parameters. The control parameters are given in tab. 3.1.6.

Parameter	*Value*
T_{nDC}	0.0023
T_{iDC}	$7.85 \cdot 10^{-5}$

Table 3.1.6: DC-control parameters

3.1.6 Reactive power control

The synthesis of the reactive power controller follows the same procedure as that of the DC-controller. The reason for this is that the system, corresponding to the imaginary part of eq. 3.1.2, contains a pole close to zero. Due to this, the pole should not be eliminated because of stability issues, and hence, the symmetrical criterion is applied. The open transfer function of the controlled system becomes:

$$\frac{i_q}{Q_{ref}} = \frac{1 + sT_{n2}}{sT_{i2}} \cdot \frac{1}{1 + s2T_{cm}} \tag{3.1.3}$$

Utilising eq. 2.4.5 and changing C with T_{pE} in eq. 2.4.6 yields the following regulator parameters, tab. 3.1.7:

Parameter	*Value*
T_{n2}	0.0023
T_{i2}	0.0047

Table 3.1.7: Reactive power control parameters

3.1.7 AC-voltage controller

The AC-control loop is supposed to keep the PCC-voltage steady. It is limited by the conditions stated in sec. 2.8.

The parameters of the voltage controller was designed so the relation between its parameters and the parameters of the reactive controller are the same as those of the relation between the I_q - and reactive controllers, and then tuned to a satisfactory response.

The parameters of the PI_{ac} are listed in tab. 3.1.8

Parameter	*Value*
T_{n3}	0.0292
T_{i3}	$9.35{\cdot}10^{-4}$

Table 3.1.8: AC-voltage control parameters

3.1.8 Active power control

The active power controller compromises a cascade of a power controller and a current controller for the DC/DC-converter. As claimed in sec. 2.11, the cascade needs to be slower than the DC-bus controller. But it should still be able to compensate power fluctuations in the grid. These are, however slow compared to the rest of the system (electric vs. mechanical time constants), and therefore, combining the two demands should not cause trouble. The parameters of the active power loop are given in tab. 3.1.9.

The parameters of the inner loop, i.e. the current controller, were calculated from the theory presented in sec. 2.12.1. The resulting parameters are given in tab. 3.1.10.

Parameter	*Value*
T_n	0.05
T_i	0.1

Table 3.1.9: Active power controller parameters

Parameter	*Value*
$L_{dc,filt}$	0.025 H
T_n	0.00125
T_i	$1.25 \cdot 10^{-5}$

Table 3.1.10: DC/DC-converter current controller parameters

3.1.9 Active damping

The active damping loop was designed based on the resonance frequency of the LCL-filter. Its purpose was to avoid the resonance problems introduced by the filter. The resonance frequency of the filter was found to be 689 Hz. To assure that the resonance frequencies were damped out, a filter constant, T_{df}=0.01 was chosen.

3.2 Discretising the control system

For digital implementation, the control system presented in 3.1 was discretised, using the theory presented in 2.14. In the following the the passing from continuous models to discret equations is presented briefly. All equations necessary for the digital control implementation are presented.

3.2.1 PI-controller

The PI-controllers are used throughout the control system. Below, in eq. 3.2.1 is the discrete PI-controller derived in [14] presented, on the form of a difference equation. u[k] is the general output variable of the PI, while e[k] is the general control error. The term [k] refers to the present value of the control variable, while the term [k-1] referes to the previous value.

$$u[k] = u[k-1] + K_p(1 + \frac{T_{st}}{2T_i})e[k] - K_p(1 - \frac{T_{st}}{2T_i})e[k-1] \qquad (3.2.1)$$

3.2.2 Digital current controller

The digital current controller is given below. The controller, which is presented in eq. 2.4.2, compromises a PI-control, together with the feed forward term of the voltage of the same axis, and the cross coupled term of the current of the opposite axis.

Implementing eq. 3.2.1 yields the following discrete controllers:

$$u_{d,ref}[k] = u_{d,ref}[k-1]+K_p(1+\frac{T_{st}}{2T_i})e_d[k]-K_p(1-\frac{T_{st}}{2T_i})e_d[k-1]+u_{d,mes}[k]-\omega l i_{q,mes}[k] \tag{3.2.2}$$

$$u_{q,ref}[k] = u_{q,ref}[k-1]+K_p(1+\frac{T_{st}}{2T_i})e_q[k]-K_p(1-\frac{T_{st}}{2T_i})e_q[k-1]+u_{q,mes}[k]+\omega l i_{d,mes}[k] \tag{3.2.3}$$

3.2.3 Secondary controllers

The secondary controllers follow the pattern of the current controllers, expect for the latter having cross-couplings and feed forward terms.

The DC-bus voltage control in discrete form is given in eq. 3.2.4.

$$i_{dc}[k] = v_{dc}[k-1] + K_p(1 + \frac{T_{st}}{2T_i})e_{dc}[k] - K_p(1 - \frac{T_{st}}{2T_i})e_{dc}[k-1] \tag{3.2.4}$$

And the reactive power controller is given in eq. 3.2.5

$$i_{q,ref}[k] = i_{q,ref}[k-1] + K_p(1 + \frac{T_{st}}{2T_i})e_q[k] - K_p(1 - \frac{T_{st}}{2T_i})e_q[k-1] \tag{3.2.5}$$

3.3 Summarising the control synthesis

In this section, the synthesis of the control system has been presented. The continuous versions of the control were used for system simulations

in PSCAD. It is worthwhile to notice the form which the continuous PI-controllers are written on. The background literature, [5] and [6] uses the form in eq. 3.3.1, and hence, this is used for the controller synthesis as well. However, a more common way to write this controller is given in eq. 3.3.2. These forms are equivalent, when setting K_p=T_n/T_i and T_n=T_i. The latter is also the base for the discrete controllers.

$$\frac{u}{i} = \frac{T_n s + 1}{T_i s} \tag{3.3.1}$$

$$\frac{u}{i} = K_p \frac{1 + T_i s}{T_i S} \tag{3.3.2}$$

The discrete equations for the system were used when implementing the control in the DSP for the laboratory work, presented in sec. 6. Some of the parts for the continuous control system were left out. This was due to limited time for laboratory work, and hence, this system was simpler than that simulated. A detailed description of this system is given in sec. 6 The different discrete control parameters were not calculated in this section, as they depend on the actual parameter values, which should be measured in the laboratory.

4 Dimensioning of the super capacitor bank

Following from the strategy for controlling the active power output from the wind farm, presented in sec. 2.13, and the choice of DC/DC-converter technology, a suitable energy storage size was estimated. This size should be large enough to provide the energy needed for compensating the power fluctuations of the wind farm, but it should also be restrained to this. Super capacitors are expensive components, and the size of the bank should be optimised.

The wind power datas used in this design example are given in fig. 4.0.1.

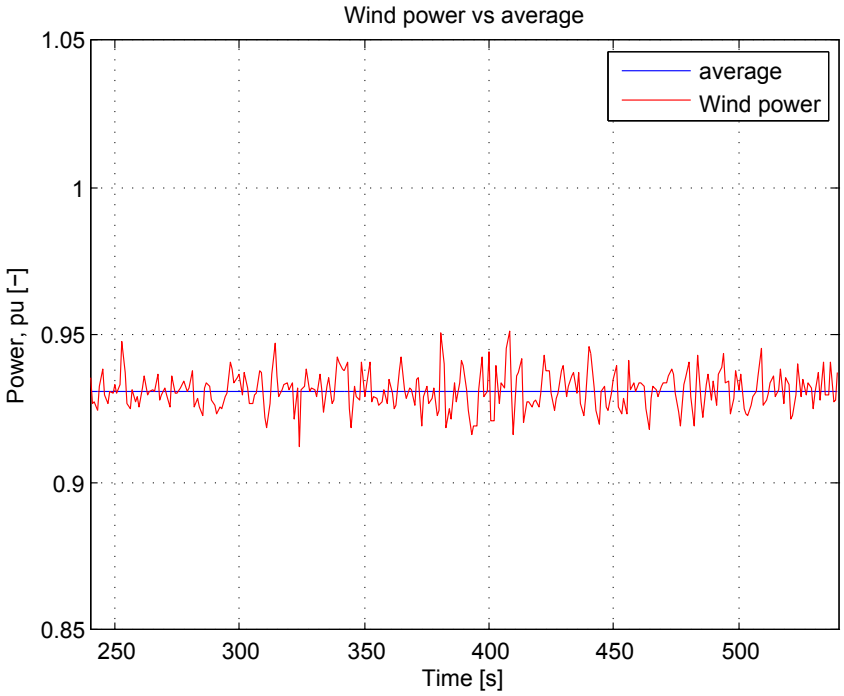

Figure 4.0.1: The output power of a wind farm

In tab. 4.0.1, key values, based upon the above presented wind power data, for the designing of the converter and the super capacitor bank are listed.

Choosing the maximum deviation from the mean value as the power rating of the DC/DC-bus converter yields the possiblity for compensating all fluctuations within the given time series, can be compensated given large enough energy storage. Normally, it would be wise to add a safety margin to this

Parameter	*Value,pu [-]*
Mean power	0.9313
Max. power	0.9519
Min. power	0.9105
Max. deviation	0.0208

Table 4.0.1: Key values, SCESS design

value. However, the design example presented here is based on a single wind turbine, and in an entire wind farm, there is a certain coincidence factor, smoothing out some of the powere fluctuations.

The design example is based on the power in a wind farm fluctuating with a frequency three times that of the rotational speed, which is due to the shadowing effect of the tower. The mechanical speed of the turbines is normally betewen 12 and 16 rpm, which leads to power fluctuations with a frequency of 0.6 to 0.8 Hz. For this example, a 100 MWA rated wind farm is used, which is a reasonable wind farm size. For estimating the energy storage, a rough integration of the deviation from the mean power value was done, based on a time step of 1 s. In addition, the integrated result was divided by a factor of four because most of the time, the wind is fluctuating rapidly around the mean value which means that the energy storage can be reduced. The system parameters found are given in tab. 4.0.2. The ESS size is takeing into consideration that using a buck-boost DC/DC-converter, 75 % of the energy can be utilised.

Parameter	*Value*
Energy needed	73.77 MJ
ESS size	98.34 MJ
Super capacitor	5.46 F
Rating, converter	2.08 MW

Table 4.0.2: Energy storage size

Using these parametres means the SCESS can, in a worst case scenario, feed the grid at full power rating of the converter for 35.46 s if the super capacitors are fully charged.

5 STATCOM/SCESS simulations

5.1 Introduction

The simulations of the whole system, including the DC/DC-converter mounted in shunt with the STATCOM, were divided in three sections. The first, using the STATCOM/SCESS only for reactive power compensation, the second one only for active compensation, and the third applying both at the same time.

The STATCOM/SCESS used in this system consisted of a LCL-filter, a three-level NPC inverter, a half-bridge buck-boost DC/DC-converter and the super capacitor bank, as depicted in fig. 5.1.1 The grid side was modeled as a weak grid, with possible fluctuating bus voltage. The wind power was introduced by a single wind turbine with induction generator directly connected to the grid, which is a common technology today. The ratings of the SCESS found in sec. 4 were reduced from the ratings of the design example of 100 MW wind farm, to the simulation system, with 2 MW wind turbine.

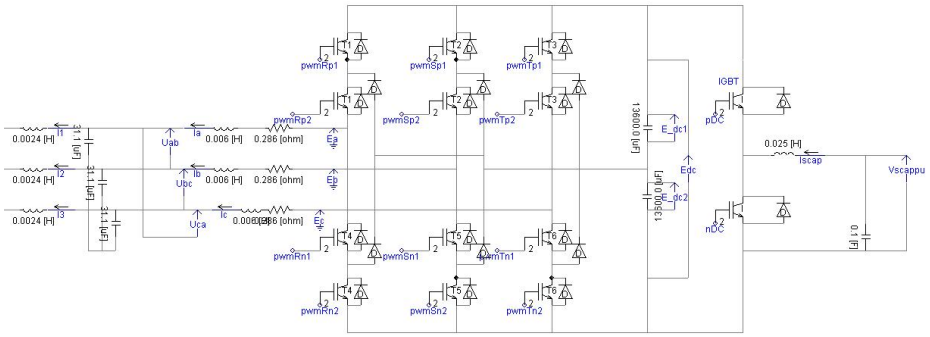

Figure 5.1.1: The STATCOM/SCESS system simulated

All the simulations were performed from steady state operation, i.e. the start up transients were not considered. For additional simulation results, see app. B.

5.2 STATCOM in reactive power compensation mode

The simulation presented in this section was carried out to document the performance of the STATCOM/SCESS system while compensating the reactive power, and hence, controlling the voltage. The voltage should be kept steady within the limits of the STATCOM's reactive power capability. If the voltage drops below this, the droop control for the grid voltage reference should be activated, and assure that controlability of the grid voltage is not lost.

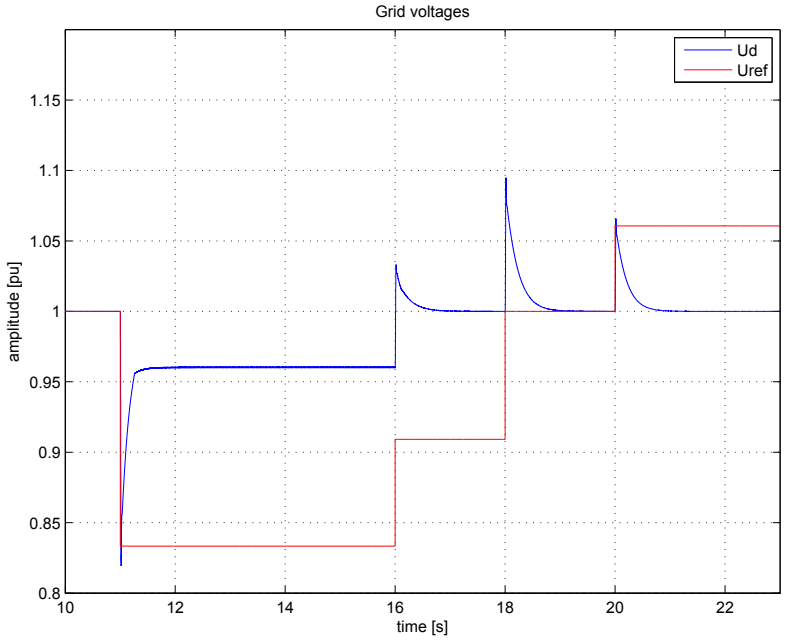

Figure 5.2.1: Grid voltage with reference

In fig. 5.2.1, the grid voltage with- (blue) and without (red) compensation is represented. As seen, with compensation, the voltage is closer to 1.0 pu, which shows that the reactive power compensation part of the STATCOM is working satisfactory. Also, the droop control is working like expected, since a major drop in the AC-bus voltage results in a less severe drop in the compensated grid voltage. This compensation results in a reactive power demand, shown in fig. 5.2.2. As seen, the reactive power is kept within the limits of the system of $\pm$ 1.0 pu.

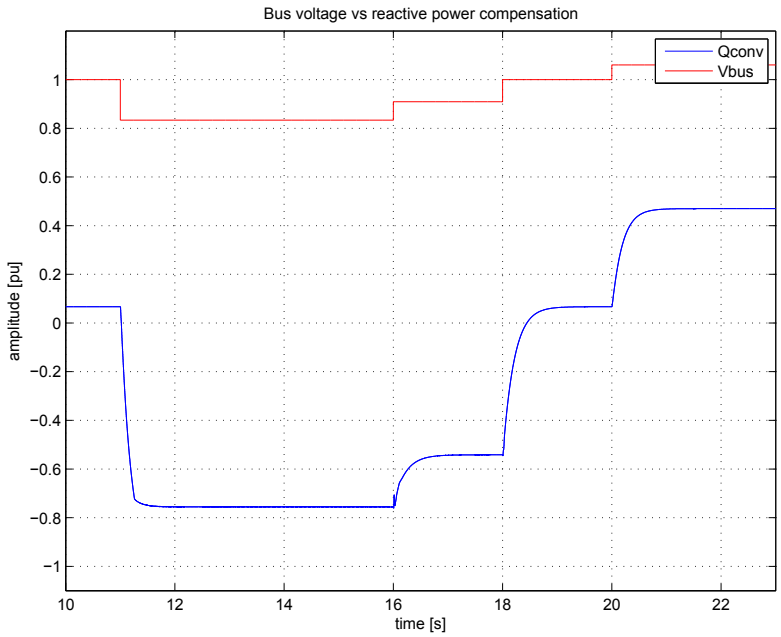

Figure 5.2.2: AC-bus voltage vs reactive power from converter

The resulting currents are given in fig. 5.2.3. As expected, the direct axis current is kept at a small value, only used to maintain the DC-bus voltage at the desired level, while the value of the quadrature axis current corresponds to the reactive power of the converter. The response of the current controller is satisfactory, with a quick, but smooth response to a change in the reference current.

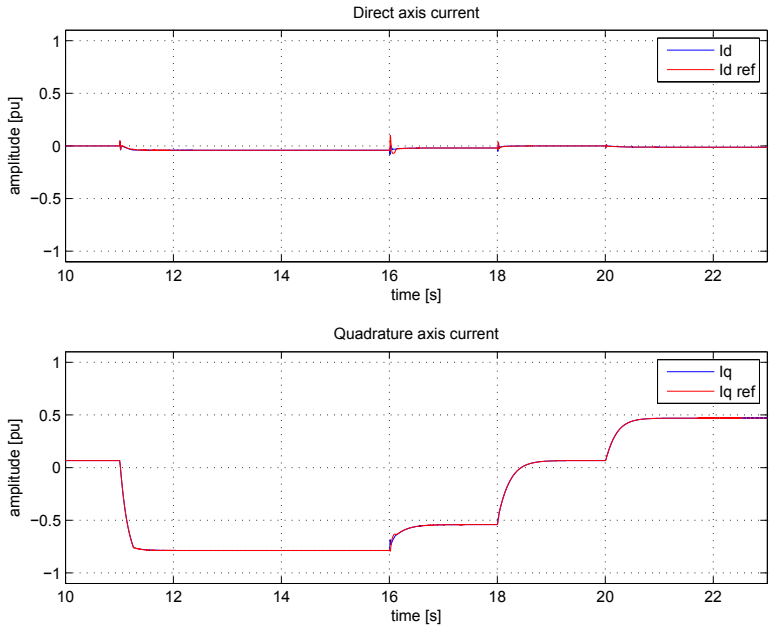

Figure 5.2.3: Converter currents in the d,q-frame

The DC-bus voltage should always be kept steady, or close to steady. In addition, the voltage should be equally shared between the two capacitor banks, in order to avoid internal over voltages and heavy current distortion due to over modulation in the switching. The DC-bus voltages are given in fig. 5.2.4. The above-mentioned demands are respected here.

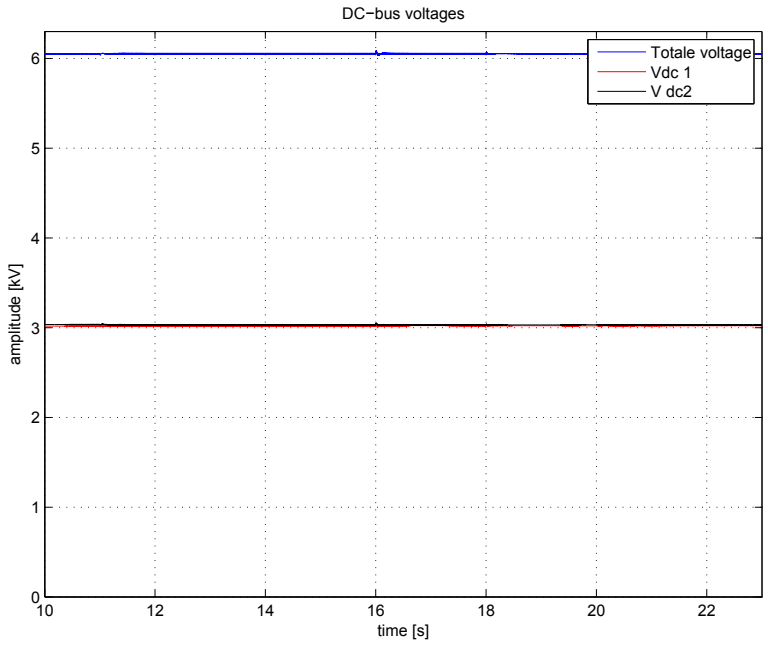

Figure 5.2.4: DC-bus voltages

The results presented in this section implies that the VSC is working satisfactory as a STATCOM with regards to the voltage stabilisation/reactive power compensation.

5.3 STATCOM in active power compensation mode

The simulations were carried out at nominal grid voltage, with no wind power connected, so the only active part of the STATCOM/SCSS system is the DC/DC-converter with its current control. However, injecting current in the grid will affect the voltage, and through this activate the reactive controller to some extent, which is set to maintain a voltage of 1.0 pu. Hence, a slight change in the reactive power should be seen when the active power is set.

The current reference of the SCESS was set to a constant value document the potential performance of the control of the buck-boost converter and the super capacitor storage alone, in an idealised case.

The DC/DC-converter's ability to follow its reference is the most important feature, as it will decide, or eventually limit, its ability to compensate the power fluctuations in the wind farm. In fig. 5.3.1, the super capacitor current is given together with its reference. The reference value applied is 1.0 pu. The functioning of the regulator and the converter is satisfactory, both regarding its ability to follow the reference in steady state, and the transient response.

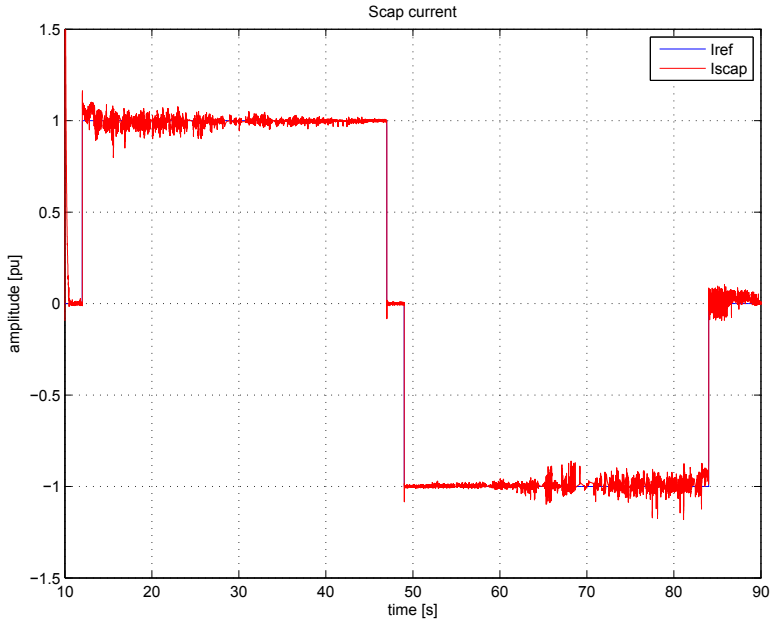

Figure 5.3.1: Reference and super capacitor current.

The current is depending on the rate of change of the super capacitor voltage, V_{scap}. This relation is shown in fig. 5.3.2. In addition, the capacity of the super capacitor bank which is 35.46 s (see sec. 4) at full power of the DC/DC-converter, is shown. Since the lower limit of the super capacitor voltage is at 0.5 pu, it is fully discharged at around 47 seconds, while the current reference was set at 12 seconds.

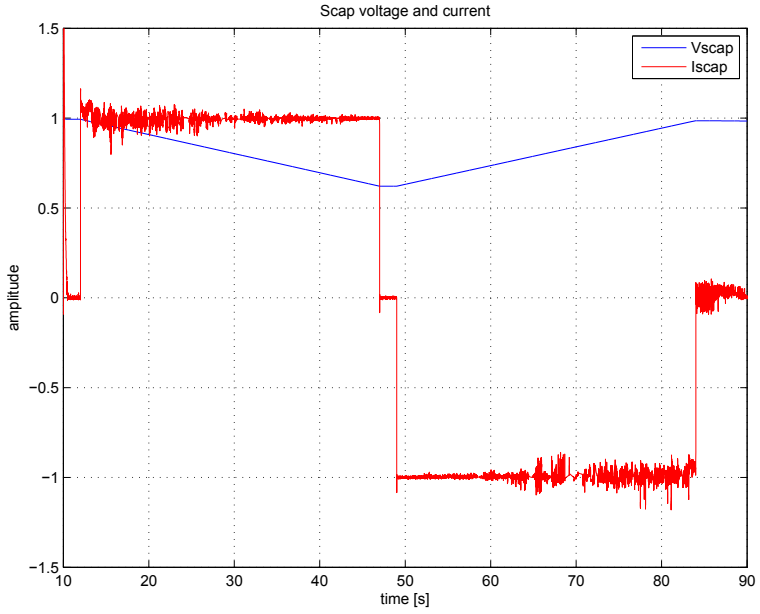

Figure 5.3.2: Super capacitor voltage vs current

The resulting currents for the VSC is given in fig. 5.3.3. I_d should be controlled in order to maintain the DC-bus voltage, and by this also controlling the active power fed to the grid from the converter.

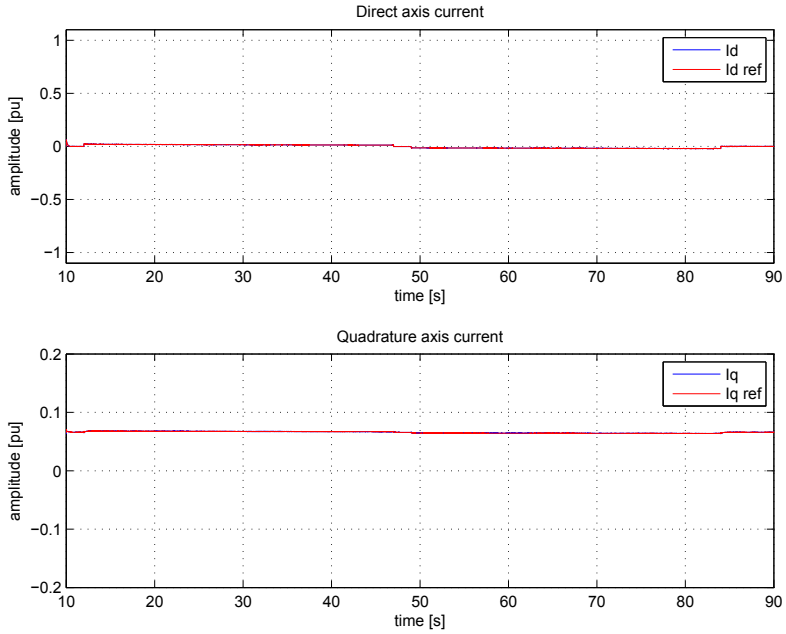

Figure 5.3.3: The currents of the VSC

As seen from the d,q-current plots, the direct axis is responding to the change in the DC-bus voltage. The increase of current injection from the converter to the grid causes a higher voltage drop in the grid, which demands for reactive compensation This is seen as a small responses of the quadrature axis current.

The transients in the DC-bus voltage should be quickly damped out when they occur due to changes in the super capacitor current injection. In fig. 5.3.4 the relation between these two variables is given, and the conclusion based on these plots is that the DC-bus controller handles transients in the voltage in a satisfactory way.

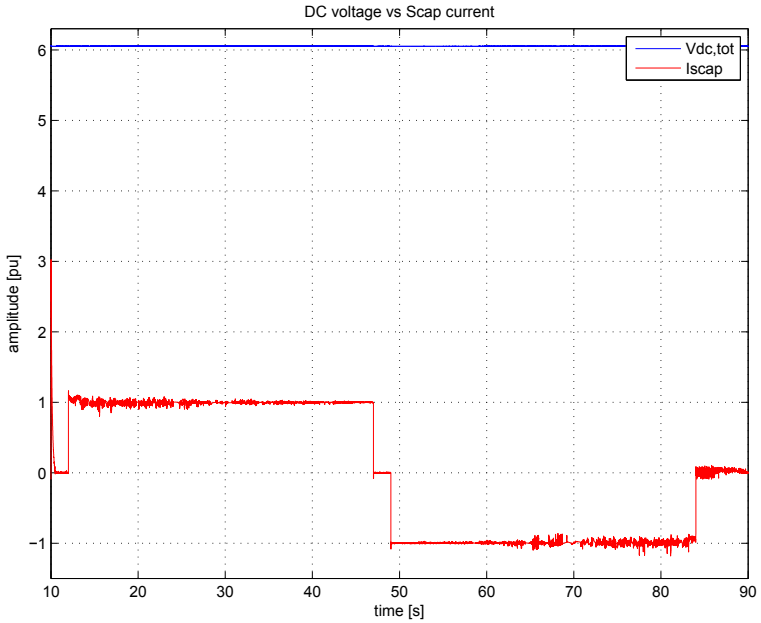

Figure 5.3.4: DC-bus voltage of the VSC and super capacitor current

5.4 Active power fluctuations compensation

The purpose of the SCESS system is to maintain the output power of the wind farm at a steady state. In the following, this ability is documented. The reference for the active power compensation part is dynamical, based on the output power of the wind farm and the voltage level of the super capacitor. The latter is introduced as a constraint, since a saturated super capacitor results in insufficient active power compensation. The simulations are carried out from a steady state, with the super capacitor partially charged.

Below, in fig. 5.4.1, the active output power from the PCC is represented together with the wind turbine power. The small power fluctuations of the latter is eliminated. The steps in the output power from the PCC is due to saturations in the super capacitor voltages, or larger steps in the wind power fluctuations. This indicates that the compensation part is working out satisfactory. However, the dynamic power reference is of some concern, since it causes, most probably, unnecessary steps in the grid power. The reason for this is most likely that the estimation does only take into account the power in the grid, and not the losses in the filter.

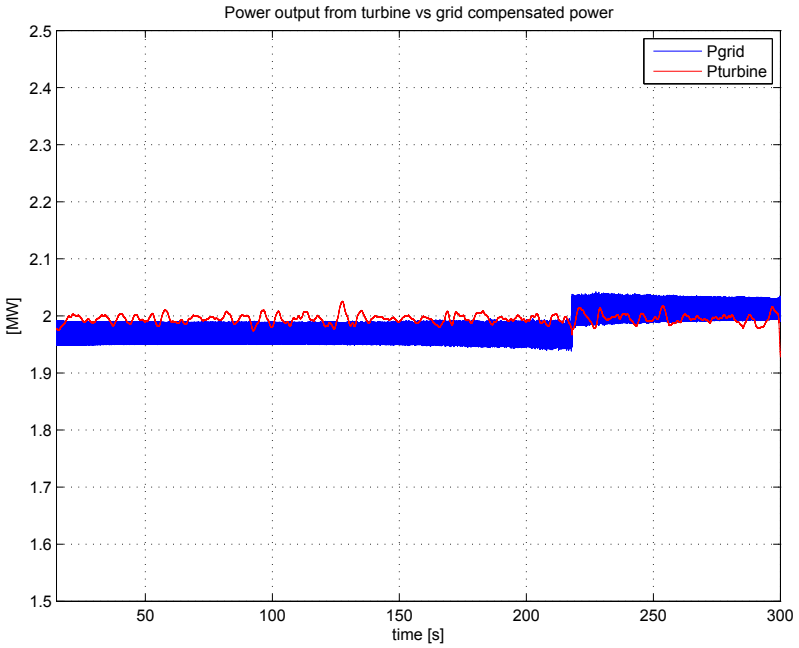

Figure 5.4.1: Active power from wind turbine and at the PCC

In fig. 5.4.2, the super capacitor voltage is given, together with its current. The main trends in the changing voltage are due to change in the active power reference, while the smaller variations are due to the fluctuations in the wind turbine power, which causes the capacitor to charge and discharge continuously. This builds up under the conclusion that the SCESS is capable of compensating the wind power fluctuations.

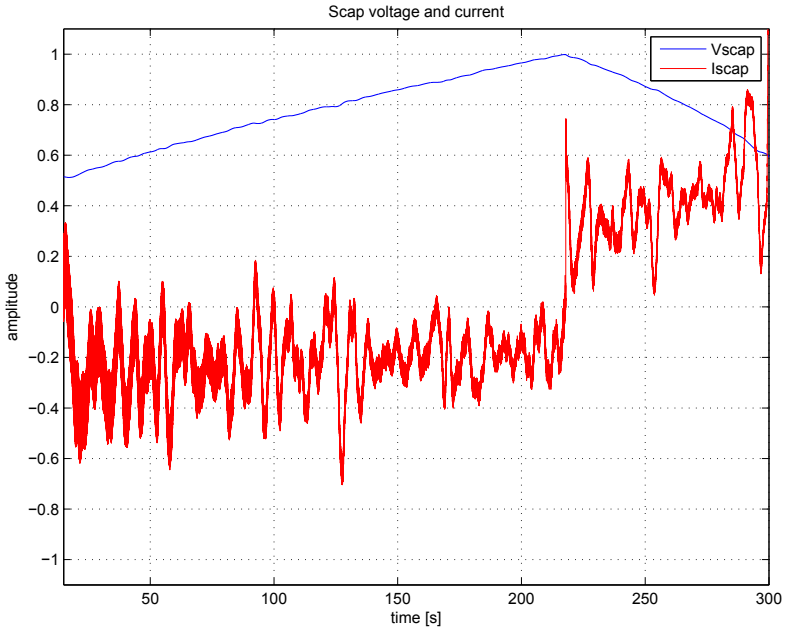

Figure 5.4.2: The super capacitor voltage and current

The active power transfer causes voltage drops, which demands for the reactive power compensation. The reactive power delivered by the STATCOM is given, together with the active power transfer from the VSC, in fig. 5.4.3. The reactive power demand is approximately 0.2 pu, which indicates the need of reactive compensation in the grid. Also, this indicates that the STATCOM/SCESS cannot operate at both maximum active and - reactive power at the same time, due to current limitations in the inverter.

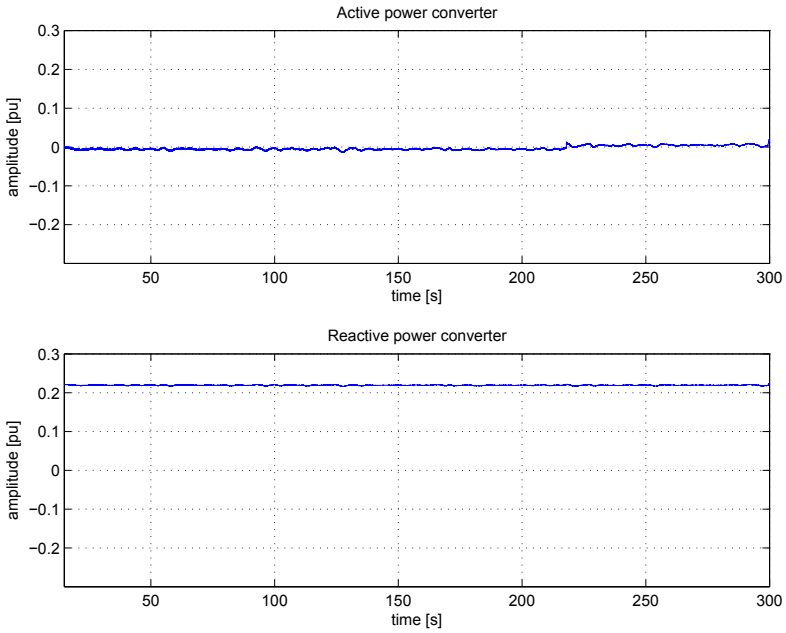

Figure 5.4.3: Active- and reactive power exchange across the VSC

5.5 Summarising the simulations

In this section, the STATCOM/SCESS system was simulated in a weak grid with wind power. The ability to maintain a stable voltage (reactive compensation), and to compensate power fluctuations have been documented. The simulations show promising results, and the device is, according to the previously presented results,showing features for which can help to improve grid integration of wind power.

6 Experimental verification

6.1 Introduction

The system treated in this work showed some promising features while being simulated. But simulations do not count for all variables, like for instance dead band time for the converter, on/off-transients in the IGBTs etc. Therefore an experimental verification of the system was performed. However, due to limited time, only the STATCOM part was tested out in the laboratory.

6.2 The model set-up

The STATCOM was built upon an existing 20 kW 3-phase 2-level laboratory converter, built by SINTEF and NTNU for the purpose of being used for different laboratory experiments. The converter uses IGBTs which can handle a current of 50 A at a switching frequency of 10 kHz. Lower switching frequencies allows higher currents. Since the model is used for testing, there are several protection devices installed in order to avoid damaging the converter. Among others; a thermal limiting switch, over current protection, DC-bus over voltage protection and an automatic dead band generator to prevent short circuiting the converter.

The DC-bus is charged with a special charging circuit, in order to avoid inrush currents when turning on the power.

The nominal voltage of the converter is 230 V rms, which results, with a Y-connected transformer, in a DC-bus voltage of 375.6 V. The DC-bus consists of two 3300 μF capacitors, which make up a stiff DC-bus. In fig. 6.2.1 and fig. 6.2.2 is the laboratory set up presented.

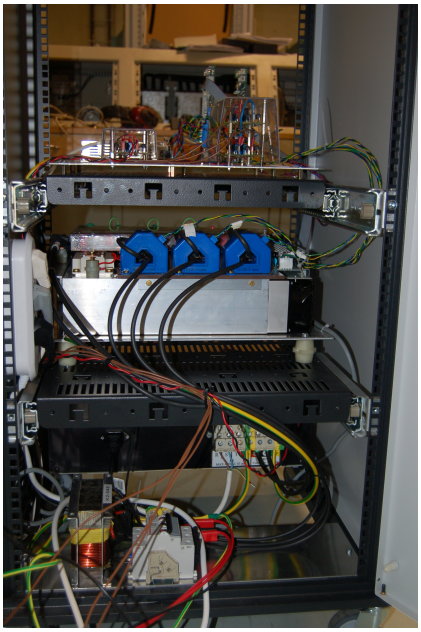

Figure 6.2.1: The front side of the converter, with current sensors and inductor filter

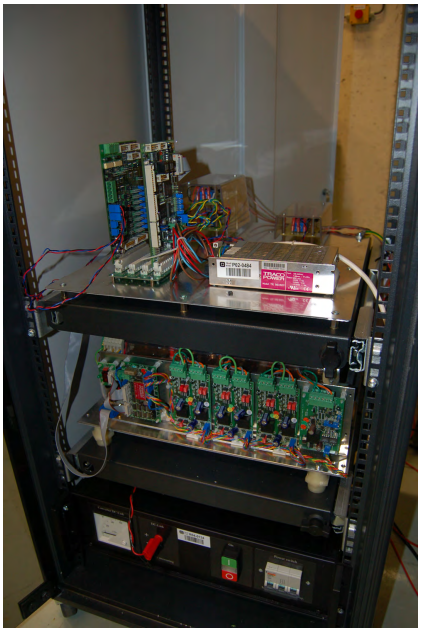

Figure 6.2.2: The back side of the converter, with driver circuits, DSP and measurement set up

The AC-filter was made of an inductor, which was measured to 0.9 mH.

The setup of the laboratory was done in a simple way, due to time limitations to the exercise. Therefore, a transformer for galvanic insulation of the circuit represented the bus, together with a large resistor in series. This resistor made the grid a simple model of a weak grid, in addition to limit the currents to a level below the level of the transformer fuses (10 A). The converter (STATCOM) was connected to the grid with an inductive filter. The most important parameters for the laboratory set up are listed in tab. 6.2.1

Parameter	*Value*
f_{sw}	5 kHz
I_n	9.16 A
U_n	230 V
$U_{dc,n}$	375.6
L_{filter}	0.9 mH
$R_{damping}$	14.5 Ω

Table 6.2.1: Paremeters, laboratory model

6.2.1 Hard- and software for the digital control

The digital controller was implemented in a Texas Instruments (TI) DSP of the type TMS320/F2812. This is a fixed point DSP operating at a frequency of 150 MHz. The DSP was mounted on a standard board used by the department of electrical engineering, constructed by Sintef/Aker Kværner. The circuit board contains the different necessary peripheral hardware for the digital control. The board is fed with a 15 V DC source, which makes the board also suitable for feeding the LEM-sensors used for current and voltage measurements.

In addition to the DSP circuit board, an extra measurement collection card was used, in order to obtain sufficient number for measurement input ports for the controller. This card is made for working with the DSP-board.

The LEM sensors used in this set up are of two different types. The ones used for voltage measurement are of the type LEM LV25-P, while the ones for current measurement are the LEM LA205-S type. The sensors were both used for measurements and realising the feed back loops of the control system. The measurements which were used were the following: Two AC line voltages in the PCC, three AC phase currents at the connection points of the converter, and a DC-bus voltage measurement. The measurements were filtered digitaly, using a first order butterworth filter with a cut-off frequency of 10 Hz. The filter constants were calculated using the Matlab signal processing toolbox function "butter".

The programming of the DSP was performed in TIs programming environment, CodeComposer Studio, v3.3. The code for the converters was written in C/C++. To implement a fully functional DSP-program, a massive amount of work is needed to understand and code the different registers and peripherals, in addition to the actual controller program. Therefore, after working a while on a program kernel, which was in no way optimal, the choice of switching to the use of a kernel offered by SmartMotor AS was taken. The SmartMotor Kernel program offers the basics needed for a DSP program, by handling interrupts, registers and setting the AD-convertion units and PWM-output pins.

Also, by using the SmartMotor Kernel, the laboratory work became a test of whether the kernel is suitable for future master works, see appendix G for a short summary of this experience. The kernel serves the user an interface which can be used for direct programming the application at higher level. That is, the kernel handles the memory mapping, register set ups and the

different interrupts for the operation of the DSP.

The program for the digital controller which was written in this work is given in appendix C.

For the operation of the DSP in real time, the ActiveDSP program was used. This was both used for operating the processor, and for logging results. The communication was set up on the serial RS-232 port, at a baud rate of 115.200.

For a full listing of the equipment and software used in the laboratory, see appendix F.

6.3 Calibration of measurements

In the kernel program, some calibrations are done in the start up of the program. However, these proved not sufficient, and additional adjustments were carried out. This was done by applying a known DC-voltage/current (for the voltage- and current sensors respectively), only including resistors in the circuit. The test current used was 3.0 A, and the test voltage was 20.0 V. Additional tuning was performed with the actual AC set up. The final calibrations which were used in the final controller are listed in tab. 6.3.1.

Measurement	*Offset*	*Scaling*
I_a	0.04	15.9
I_b	0.20	15.6
I_c	-0.05	15.3
U_{ab}	-2,67	6.741
U_{bc}	-2.21	6.819
U_{dc}	-4.28	96.21

Table 6.3.1: Calibration of LEM sensors.

6.4 Results from the laboratory model

The results of the laboratory work is divided in three parts. As the STATCOM should be able to compensate the reactive power both operating as inductive and capacitive element, an artificial reactive power reference of $\pm$ 0.2 pu was introduced. In addition, a zero reactive power case was tested.

The major results are given below, plots of more details are given in appendix D for a more thorough documentation of the controllers.

6.4.1 Reactive power = -0.2 pu

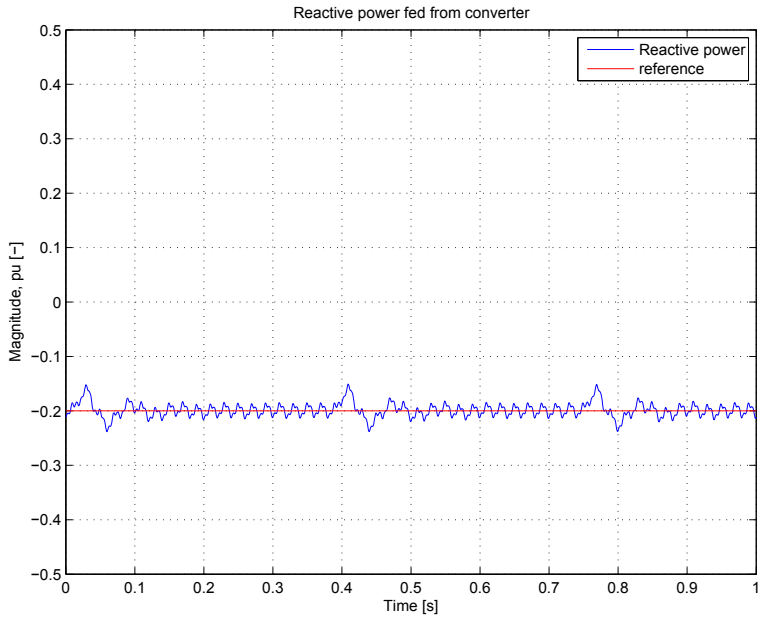

Figure 6.4.1: Reactive power fed from the converter

The ability of following a reactive power reference, fig. 6.4.1, for the converter appears as satisfactory. Some fluctuations are still left in the reactive power, but they are sentered around the reference, and hence, of no major concern. Also, being kept stable for the time span seen here implies that the controller is steady state stable, as this period corresponds to 50 times the fundamental frequency of the system (50 Hz).

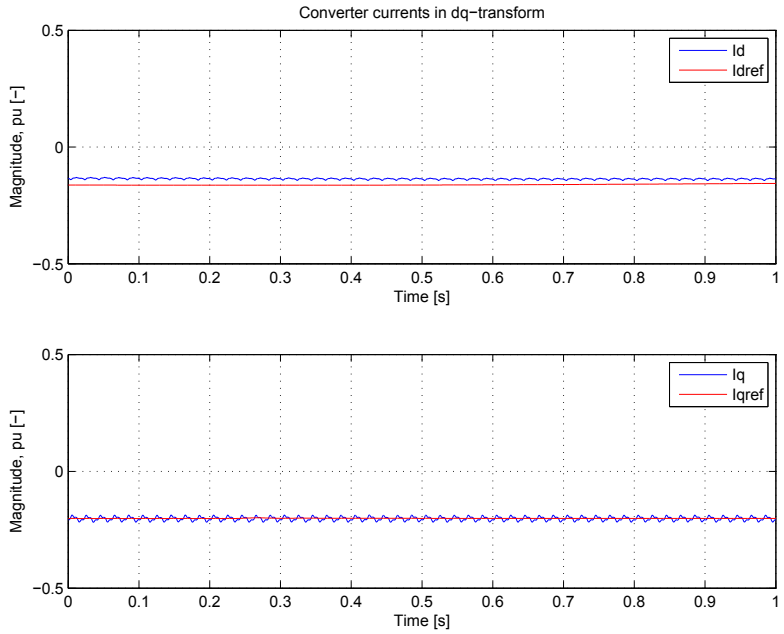

Figure 6.4.2: Direct- and quadrature axis currents of the converter

The currents of the converter, fig. 6.4.2, are following their reference in a satifsfacotry way. However, there is a steady state deviation in the direct axis current. Most likely, this is due to the feed forward term of the multivariable PI-controller not working out properly. The background for this assumption is that the quadrature axis control is following its reference with no steady state deviation, which indicates that the integral part of the control is functioning.

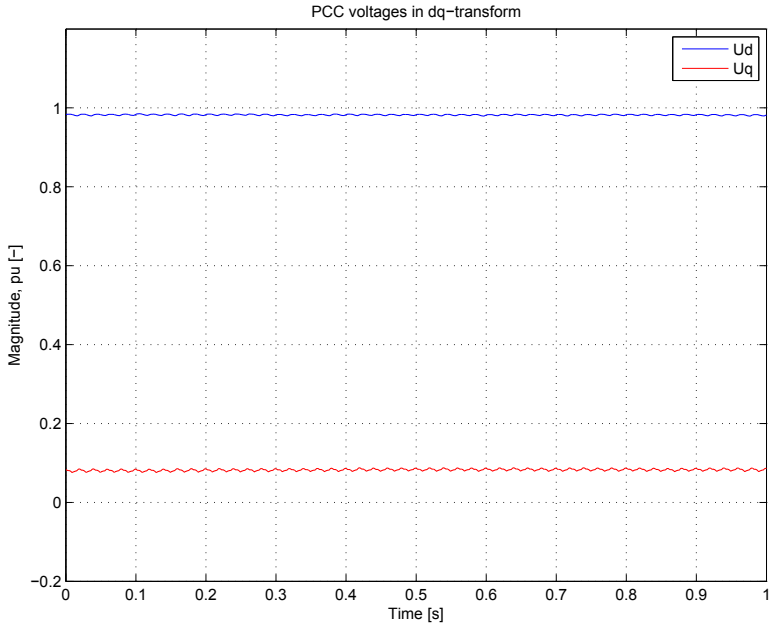

Figure 6.4.3: Voltages at the PCC

As seen from fig. 6.4.3, the voltage at the PCC of the model is steady with regards to the direct axis voltage. The quadrature axis, however, should normally be expected to be zero, as this is the point the phase locked loop locks to. The reason why it is not so, can be seen in the comparison of the grid phase voltage and the estimated angle from the PLL (fig. D.1.1. Because the PLL does not lock perfectly on the phase voltage, the quadrature axis will be different from zero.

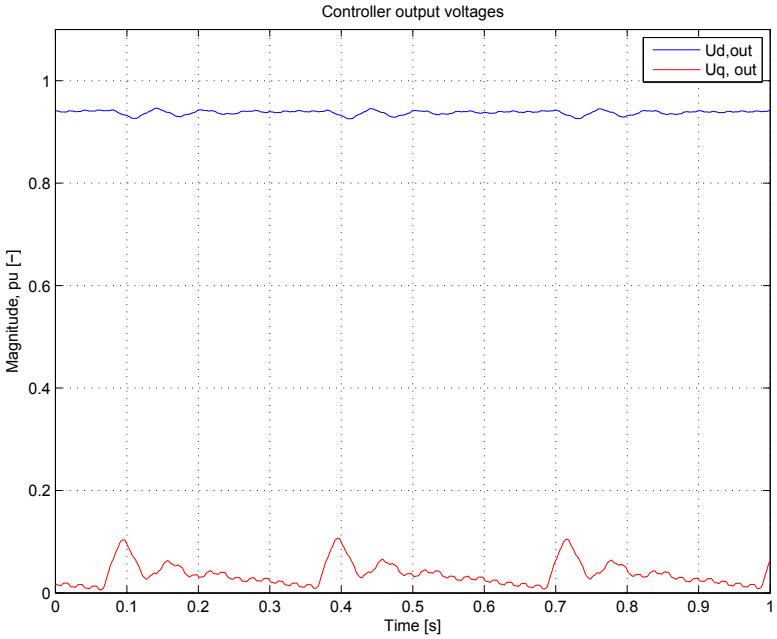

Figure 6.4.4: Reference voltages for the PWM-generator

The voltages used for generating the PWM-signals for the converter are seen in fig. 6.4.4. U_d decides the amplitude, while U_q decides the angle, and hence, the reactive power fed from the converter. The voltages, being output from the current control loops, are reflecting the above given results. As the direct axis is based on the DC-bus voltage, which is kept constant, it is kept constant as well. The reactive voltage is stable, but periodically fluctuating.

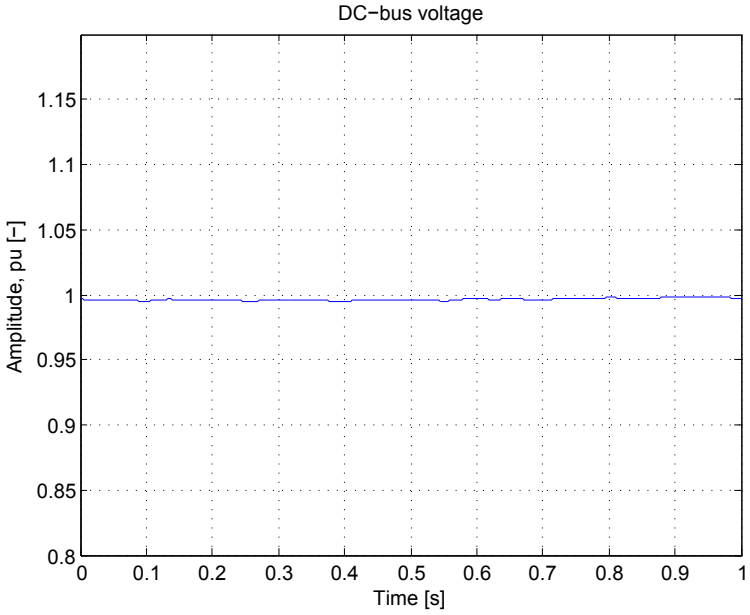

Figure 6.4.5: DC-bus voltage level

The DC-bus voltage controller is maintaining the DC-bus at a constant voltage level, fig. 6.4.5, and is by this having a satisfactory response.

6.4.2 Reactive power = 0.2 pu

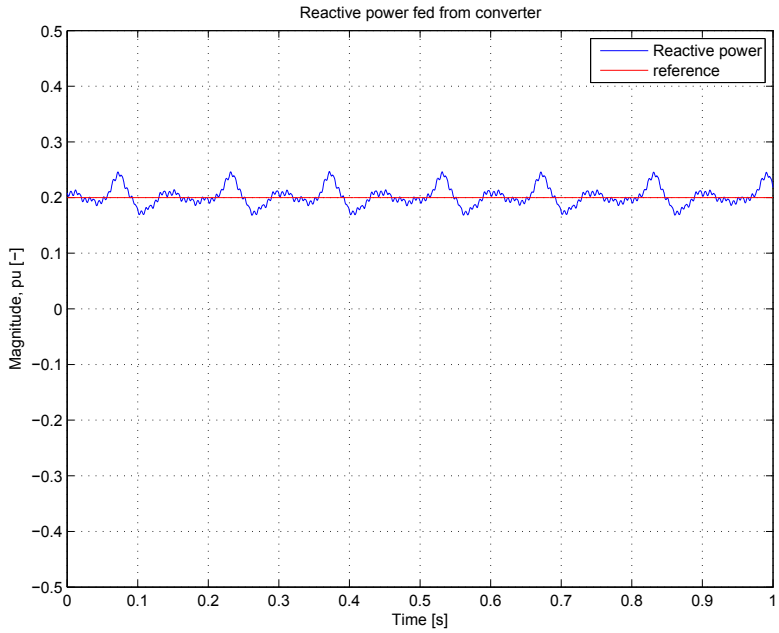

Figure 6.4.6: Reactive power fed from the converter

As for the case of a compensation of -0.2 pu reactive power, the reactive power is kept stable around its reference (fig. 6.4.6). The fluctuations are at the limit of the acceptable as the peaks are deviating considerably from the mean value, but in the principle, the controller compensates according to the demand.

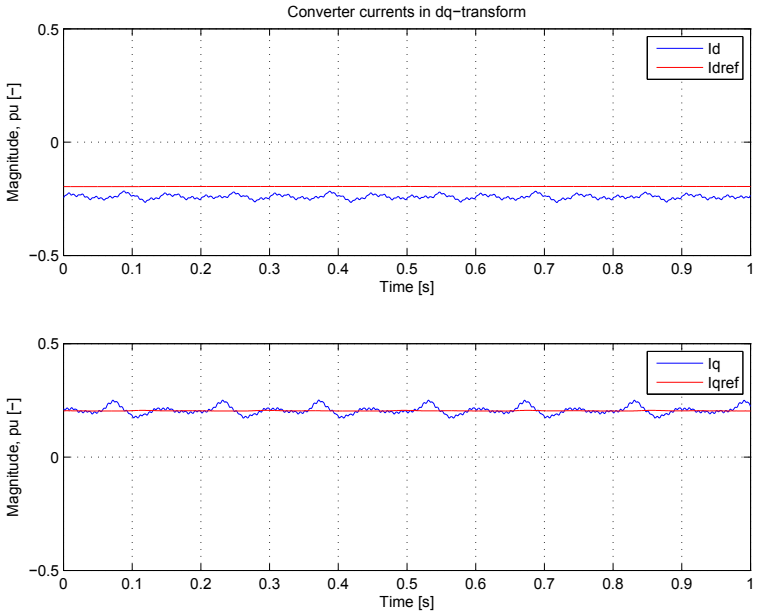

Figure 6.4.7: Direct- and quadrature axis currents of the converter

Fig. 6.4.7 gives the currents of the converter. In the quadrature axis current, the ripples of the reactive power is found. Hence, the problem is likely to be caused by the current control loop. As seen, the problem with the direct axis current having a constant deviation from its reference is refound here, only the sign of the deviation is changed. This is consistent with the case presented in sec. 6.4.1. Hence, the behaviour of the current control does not seem to depend on the operating point of the converter.

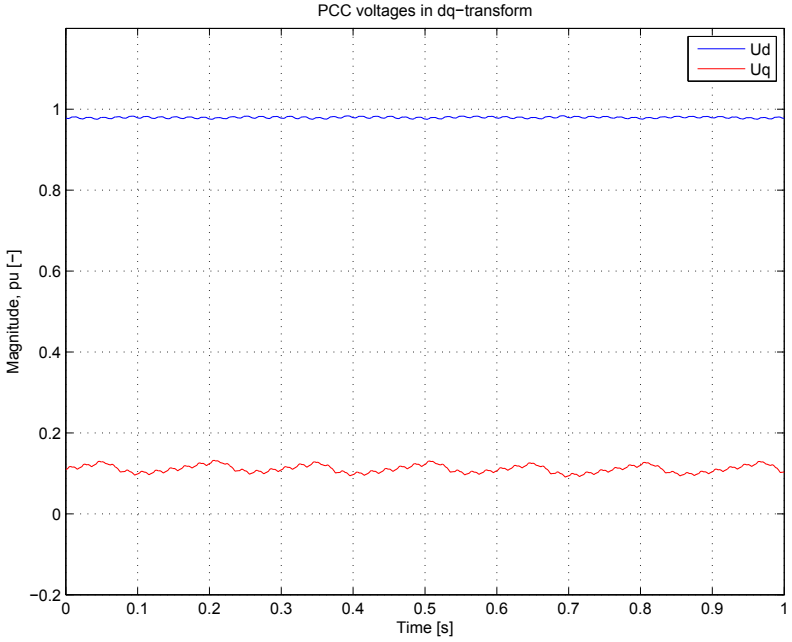

Figure 6.4.8: Voltages at the PCC

For the grid voltages, in this case it is worthwhile notising the fluctuations in the quadrature voltage. These are most likely influenced by the fluctuations in the reactive power.

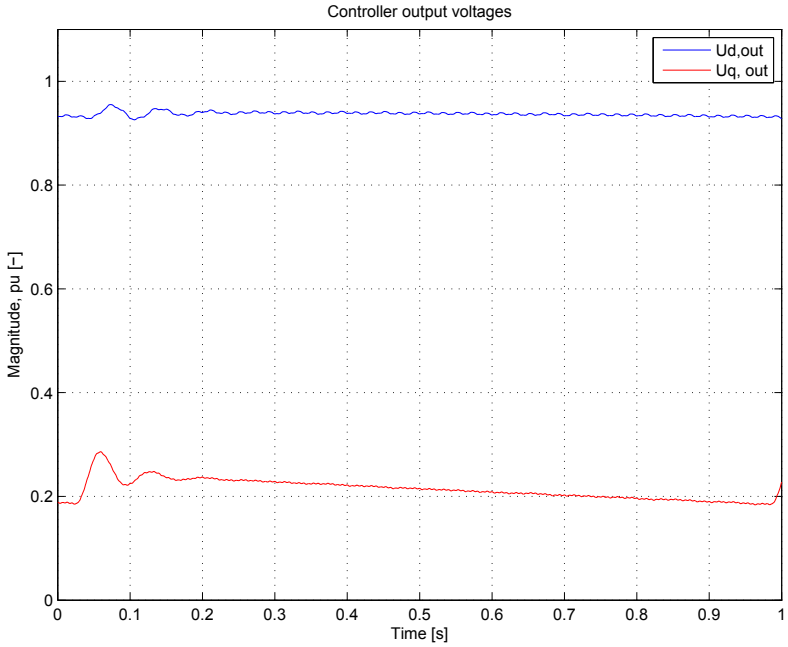

Figure 6.4.9: Reference voltages for the PWM-generator

In the converter voltages, the quadrature axis does have a damping of transients which is not favouarble. Oscilations will cause transients in the converter voltages, but the controller should be able of damping this out quickly. The bad damping time could be a problem when facing a grid with more fluctuations than the one used in this work.

6.4.3 Reactive power = 0.0 pu

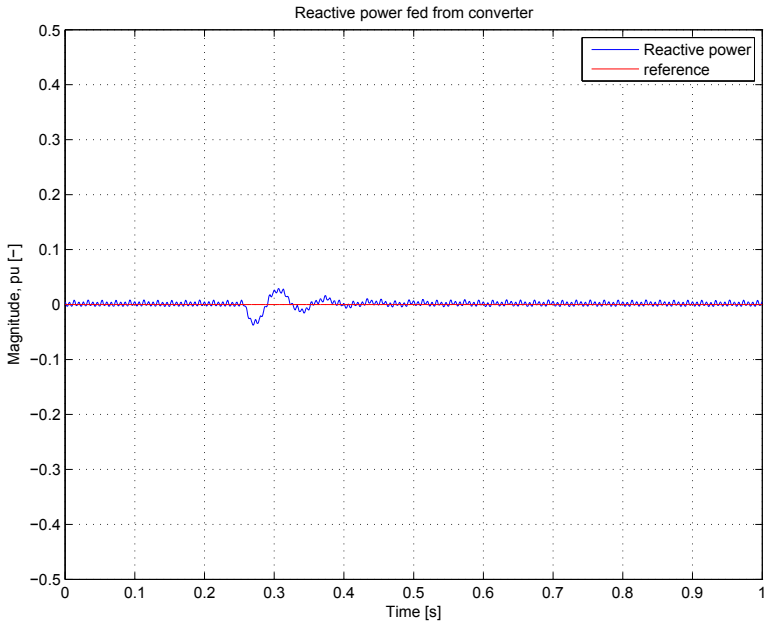

Figure 6.4.10: Reactive power fed from the converter

From fig. 6.4.10, the zero reactive power case is given. As seen, only small ripples make the grid reactive power deviate from its reference. This is satisfactory behaviour of the reactive control loop.

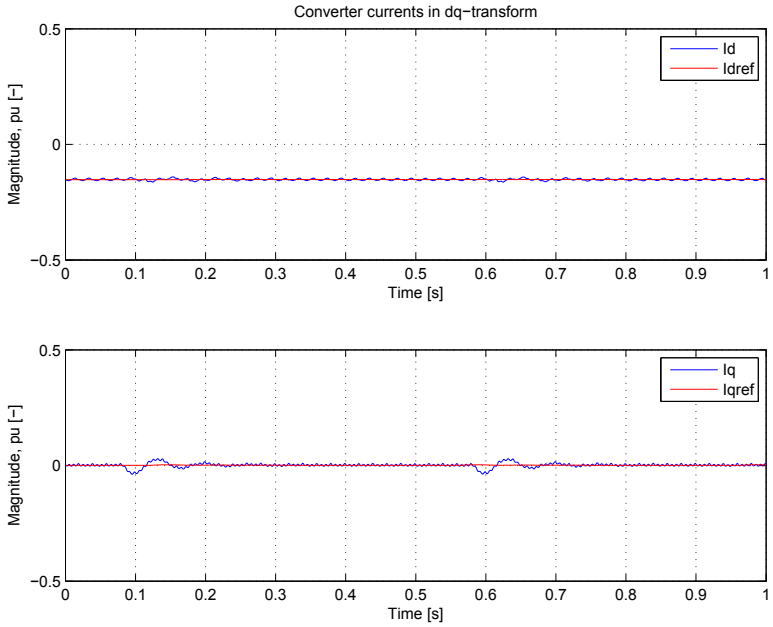

Figure 6.4.11: Direct- and quadrature axis currents of the converter

In the fig. 6.4.11, the current responses of the converter can be seen. In the discussion in the two previous sections, a small steady state deviation in I_d was commented on. This is not present here, and hence, it strengthens the suspicion of this being a problem with the cross coupled feed forward terms of the current controllers. However, I_q is satisfactory controlled.

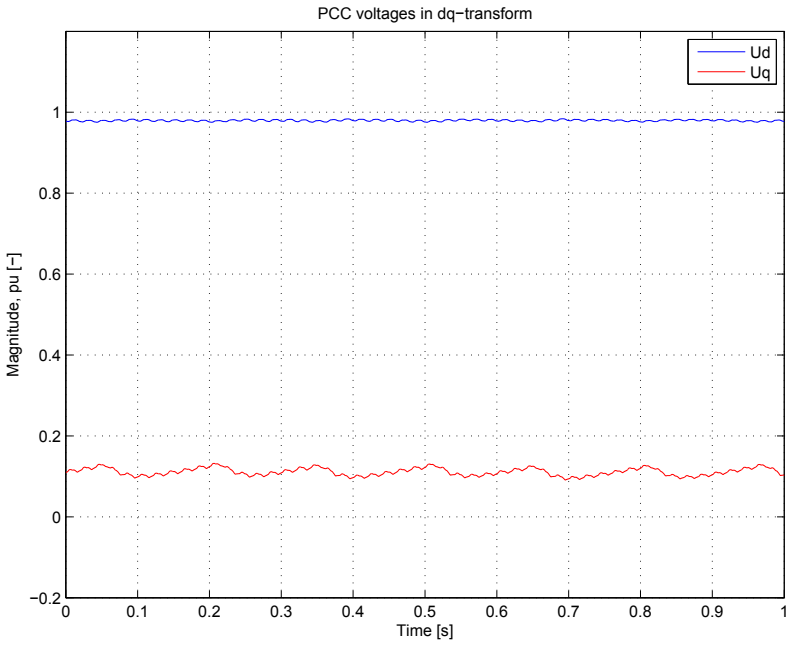

Figure 6.4.12: Voltages at the PCC

The grid voltages fig. 6.4.12 are as already mentioned deviating some from the expected zero value of the U_q. Being so in all the three cases builds up under the theory that the problem is due to the implemented PLL.

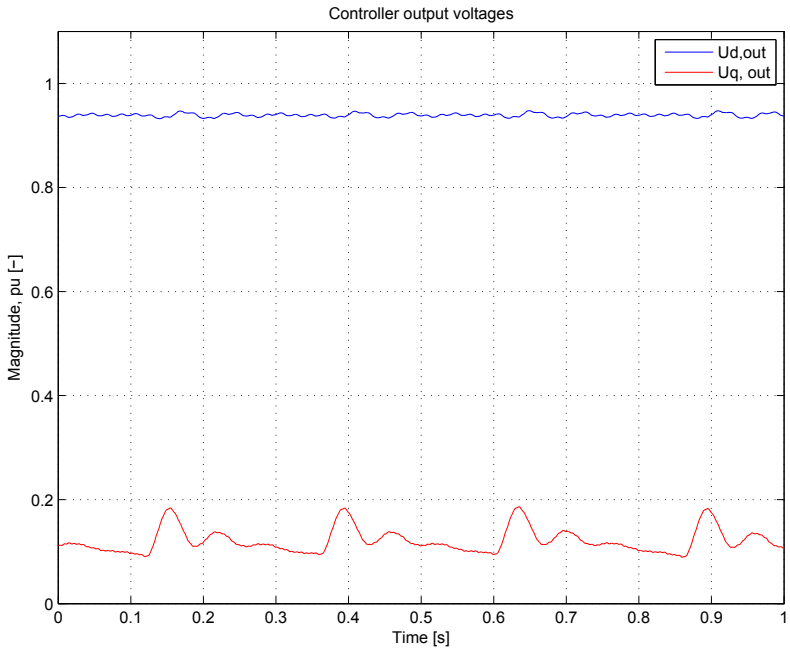

Figure 6.4.13: Reference voltages for the PWM-generator

The output of the current controllers, fig. 6.4.13 is good regarding the direct axis. The quadrature axis voltage is however fluctuating. A more constant value would have been favourable considering the stability of the system.

6.5 Discussion on the results of the laboratory work

The results from the laboratory work presented in the previous sections lead to some conclusions regarding the system in general. First, the digital control of the system is, in general, working like expectation based on the simulations. The responses of the control loops are, however not very well tuned, and more attention to the parameters of the system, and also the practical set up would have been favourable. This would lead to better responses, and most probably less fluctuations.

Second, the series coupled resistor causes the direct- and quadrature axis to be closer connected than what was seen in the simulations. Removing this would lead to better decoupling, and less charging current, I_d, for the converter. Also, the reactive power compensation capability would be improved. This will however, demand for an algorithm for synchronising the converter with the grid, which there was no time to implement in this work.

Third, the tests performed here were all steady state. Transient tests of the STATCOM should have been performed, together with an implemented AC-voltage controller and the droop control included in the simulations. But, as with the synchronising algorithm, there was no time for doing so.

At last, the SCESS part of the system was not considered at all. Carrying out an implementation of this part, in a more realistic grid model would have been desirable, but time consuming

7 Conclusion

A STATCOM/SCESS system with its control system has been designed for the purpose of improving the power and voltage quality for grid connection of offshore wind farms. The control system was designed and a method for estimating the SCESS size from wind power data was proposed. Further on, the system was simulated using the EMTDC program PSCAD. Here, a detailed model of the system was implemented, compromising a 3-level NPC converter for the STATCOM, and a half-bridge buck-boost DC-converter for the super capacitor system.

The simulatios of the system showed promising features for the STATCOM/SCESS in wind application, both with regards to the reactive power compensation part (and hence the voltage stabilising ability), and the active power flickering. However, the implemented dynamical active power reference for the SCESS was not working out as good as expected.

For the laboratory work, only the STATCOM part of the system was implemented, due to limited time. The results from this practical implementation showed the same general patterns as those of the STATCOM simulations, expect the controllers not being tuned to a response of the same level of accuracy as those found in the simulations.

8 Scope of further work

For a future work on the system presented here, some points should be paid more attention to than what was done here. The estimation of the super capacitor bank size was done in a quite rough manner. Including grid codes, and taking into acount more wind datas is recommended.

As shown in the simulations, the dynamical active power reference is not satisfactory, and more attention should be paid to this. In [10], a reduced VA-rated half-bridge converter is presented. This could be of interest for the STATCOM/SCESS, as reduced requirements for the IGBTs would lead to an overall cheaper device.

In the end, a full model of the system should be implemented in the laboratory.

References

[1] $http://themes.eea.europa.eu/Sectors_and_activities/energy/indicators/EN01, 2007.04$

[2] $http://ec.europa.eu/environment/climat/climate_action.htm.$

[3] M. Barnes A. Arumpalam and J.B. Ekanayake N. Jenkins. Power quality and stability improvement of wind farm using statcom supported with hybrid battery energy storage. *Generation, Transmission and Distribution, IEE Proceedings, vol. 153*, 2006.

[4] B.J. Barnet and L.P. Haines. High power dc-to-dc converter for supercapacitors. *IEEE INternational Electric Machines and Drives Conference*, 2001.

[5] Hansruedi Bühler. *Réglage de systèmes d'Électronic de Puissance, Volume 1: Théorie*. Presses polytechniques et Universitaires Romandes, 2006.

[6] Hansruedi Bühler. *Réglage de systèmes d'Électronic de Puissance, Volume 2: Entraînements réglés*. Presses polytechniques et Universitaires Romandes, 2006.

[7] C. Bohn and D.P. Atherton. An analysis package comparing pid antiwindup strategies. *IEEE Control systems Magazine, Volume 15, issue 2*, 1995.

[8] M. Aten C. Banos and T.C. Green P. Cartwright. Benefits and control of statcom with energy storage in wind power generation. *The 8th IEE International Conference on AC and DC Power Transmission, ACDC 2006*, 2006.

[9] Andrés Feijóo and Jos Cidrás. Analysis of mechanical power fluctuations in asynchronous wec's. *IEEE Transaction on Energy Conversion, Volume 14, Issue 3*, 1999.

[10] T.M. Undeland G. Guidi and Y. Hori. An optimized converter for battery-supercapacitor interface. *IEEE Power Electronics Specialists Conference, 2007 - PESC 2007.*, 2007.

[11] William Gullvik. Modelling, analysis and control of active front end (afe) converter. *PhD-Thesis NTNU*, 2007.

[12] Temesgen M. Hailelassie. Control of multiterminal vsc-hvdc (mtdc) systems. *Master thesis, NTNU*, 2008.

[13] Hadi Saghafi Hamid R. Karshenas. Basic criteria in designing lcl filters for grid connected converters. *IEEE International Symposium on Industrial Electronics*, 2006.

[14] Trond Andresen Jens G. Balchen and Bjarne A. Foss. *Reguleringsteknikk*. Institutt for teknisk kybernetikk, NTNU, 2008.

[15] Josep Pou Jordi Zaragoza, Salvador Ceballos, Eider Robles, Carles Jaen, and Montse Corbalan. Voltage-balance compensator for carrier-based modulation in the neutral-point clamped converter. *IEEE Transactions on Indutrial Electronics, Vol. 56, Issue 2*, 2009.

[16] Roland Longchamp. *Commande Numerique de systèmes dynamiques: Cours d'automatique*. Presses polytechniques et universitaires Romandes, 2006.

[17] Richard Lund. Multilevel power electronic converters for electrical motor drives. *PhD-Thesis NTNU*, 2006.

[18] Hamid Gualous Mamadou Baïlo Camara and Alain Berthon Frederic Gustin. Design and new control of dc/dc converters to share energy between supercapacitors and batteries in hybrid vehicles. *IEEE TRANSACTIONS ON VEHICULAR TECHNOLOGY, VOL. 57, NO. 5*, 2008.

[19] Tore Undeland Marta Molinas, Jon Are Suul. Wind farms with increased transient stability margin provided by a statcom. *CES/IEEE 5th International Power Electronics and Motion Control Conference, 2006. IPEMC '06.*, 2006.

[20] William P. Robbins Ned Mohan, Tore M. Undeland. *Power electronics*. John Wiley & Sons, Inc., 2003.

[21] Mark SUMNER Phinit SRITHORN and Ram PARASHAR Liangzhong YAO. The control of a statcom with supercapacitor energy storage for improved power quality. *CIRED Seminar SmartGrids for Distribution, 2008. IET-CIRED*, 2008.

[22] Jon Are Wold Suul. Control of variable speed pumped storage hydro power plant for increased utilization of wind energy in an isolated grid. *Master thesis, NTNU*, 2006.

[23] Jon Are Wold Suul. Method proposed during discussions on the present work. *Meeting to discuss project related problems.*, 2008.

[24] Temesgen M. Hailelassie Marta Molinas Tore Undeland. Multi-terminal vsc-hvdc system for integration of offshore wind farms and green electrification of platforms in the north sea. *NORPIE*, 2008.

[25] Vikram Kaura Vladimir Blasko. A novel control to actively damped resonance in input lc filter of a three-phase voltage source converter. *IEEE Transactions on Industry Applications, Vol. 33, Issue 2*, 1997.

[26] Dianguo Xu Yongqiang Lang and Hongfei Ma Hadianamrei S.R. A novel design method of lcl type utility interface for three-phase voltage source rectifier. *IEEE 36th Power Electronics Specialists Conference, 2005. PESC '05.*, 2005.

[27] Subbashish Bhatttacharaya Zhengping Xi, Babak Parkhideh. Improving distribution system performance with integrated statcomm and supercapactior energy storage system. *IEEE Power Electronics Specialists Conference, 2008. PESC 2008*, 2008.

A PU-system

The PU-system utilized in this work is given below.

U_n=U_{ll}

$$U_b = \frac{\sqrt{2}}{\sqrt{3}} U_n \tag{A.0.1}$$

$$I_n = \frac{S_n}{\sqrt{3} U_n} \tag{A.0.2}$$

$$I_b = \sqrt{2} I_n \tag{A.0.3}$$

$$Z_{base} = \frac{U_n^2}{S_n} \tag{A.0.4}$$

$$U_{dc,base} = 2 U_b \tag{A.0.5}$$

B Additional simulation results

In the chapter presenting the simulation results, only the most important results were presented. Some additional results could be interesting for the documentation of the system operation. These are briefly presented in this appendix.

B.1 STATCOM in reactive power compensation mode

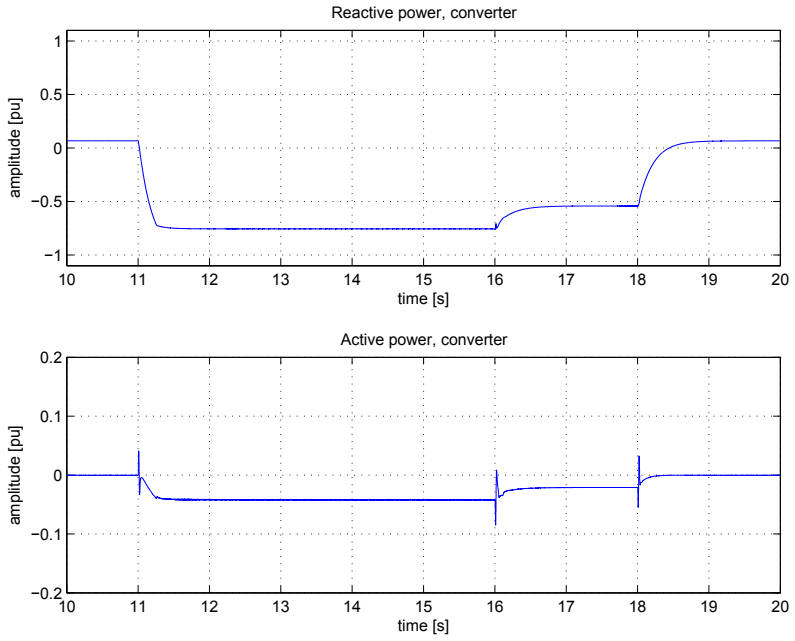

Figure B.1.1: Active- and reactive power exchange in the VSC

In fig. B.1.1, the power exchange across the VSC is presented. The converter exchanges only a small amount of active power, enough to maintain the DC-bus voltage constant. The reactive power exchange is higher, due to the drop in voltage. Howevere, as seen, the device is not utilising its full reactive power capability. Hence, the controlability of the grid voltage is preserved.

The outcome of the active damping of the current controller is given in fig. B.1.2.

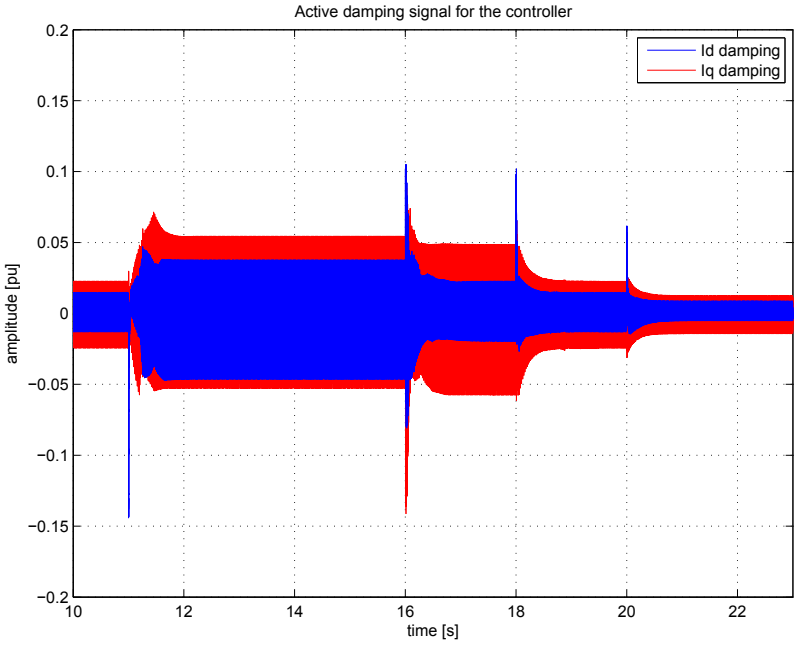

Figure B.1.2: Active damping currents

B.2 STATCOM in active power compensation mode

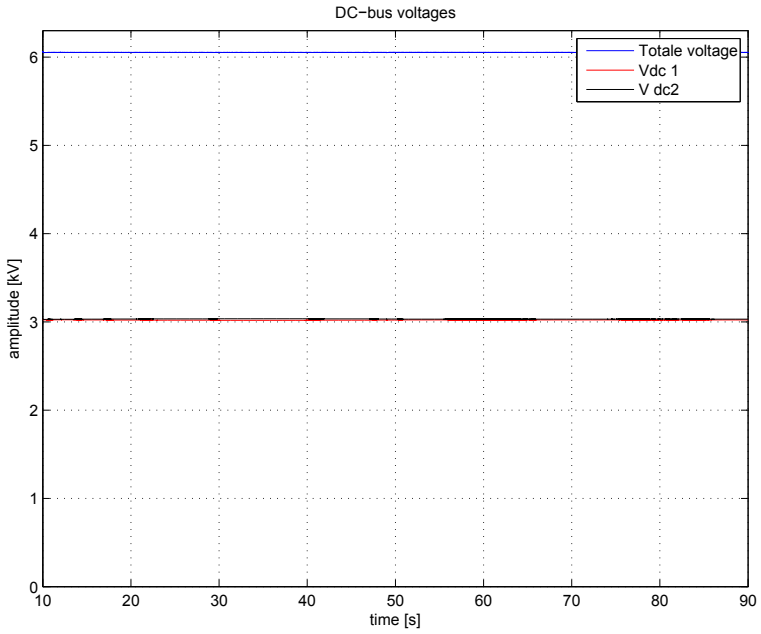

Figure B.2.1: The DC-bus voltages of the STATCOM

The DC-bus voltages are given in fig. B.2.1.As seen, the voltages are kept steady and balanced during the whole operation of the STATCOM/SCESS.

B.3 Active power fluctuations compensation

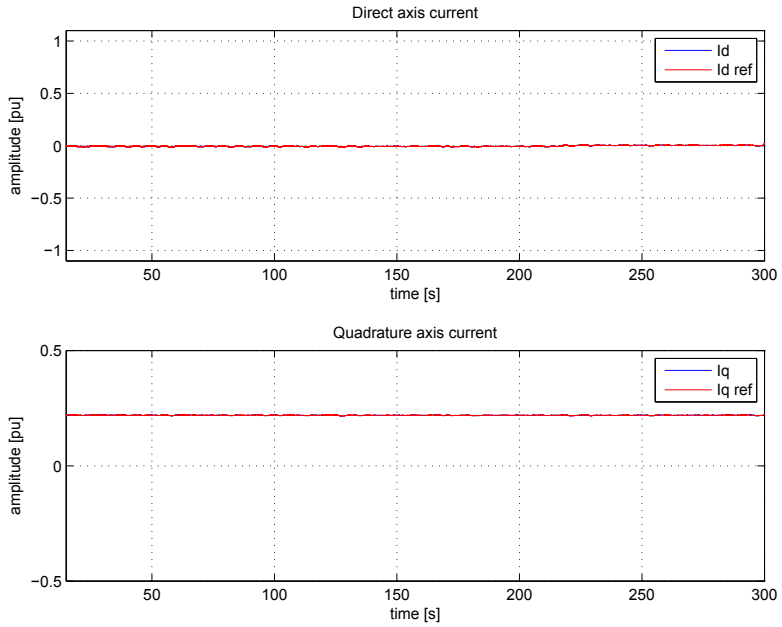

Figure B.3.1: The converter output currents

The direct- and quadrature axis converter currents are given in B.3.1. The direct axis current is slighlty changing due to the wind power fluctuations, while the reactive power is at a higher level, meaning that the converter is operating in compensation mode.

As seen from B.3.3, the grid voltage is maintained steady, at 1 pu during the whole time span.

The DC-bus is kept steady, as expected, based on the fact that the high current injections applied in 5.3 only led to small changes.

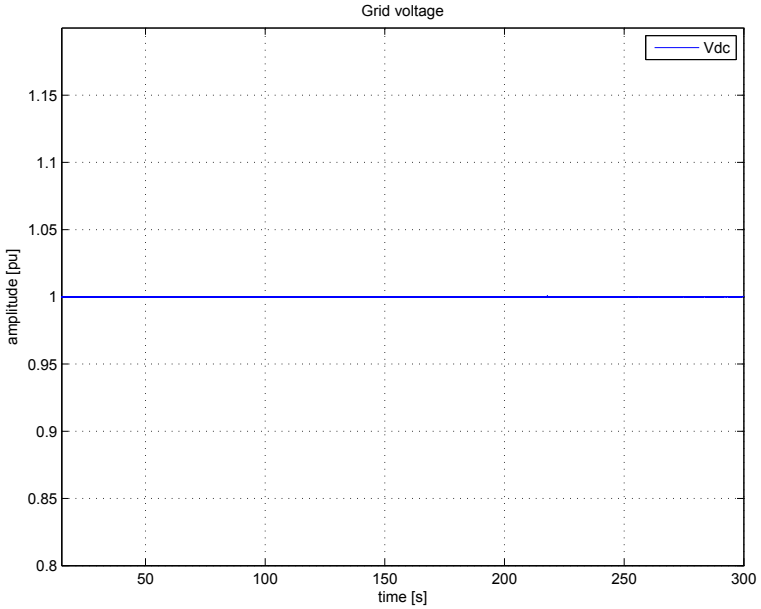

Figure B.3.2: Grid voltage at PCC

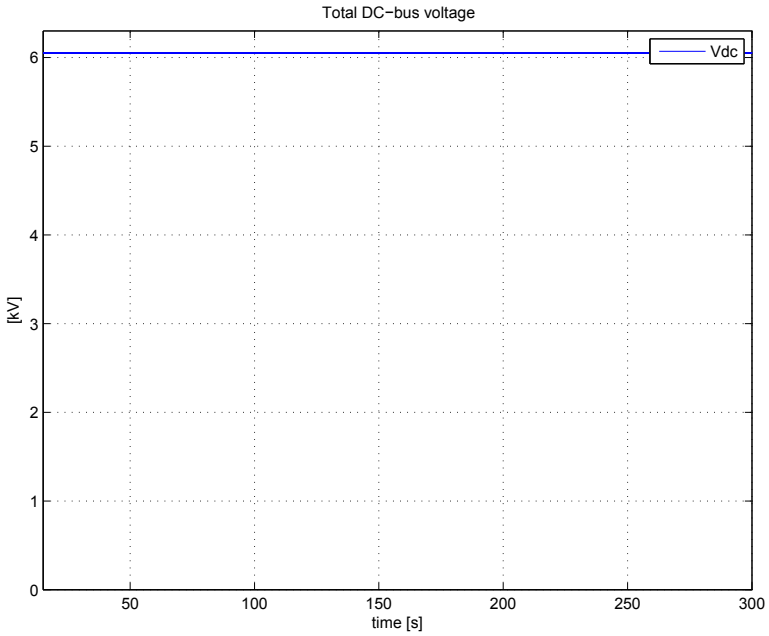

Figure B.3.3: DC-bus voltage

C DSP program used in practical implementation

In the following, the DSP program part written especially for this work is given. The rest of the program, being restricted by copyrights etc, is left out.

C.1 Interrupt program

```
//Auquiring␣the␣measurement␣datas
//adjusting␣to␣obtain␣zero␣offset.

I3ph[0]=Inverter::detail::st.curr[0]-_IQ12(0.40); //Including␣LEMA-offest
I3ph[0]=_IQ12div(I3ph[0],_IQ12(16.275)); //Scaling␣4.968*1.3
I3ph[1]=Inverter::detail::st.curr[1]-_IQ12(0.0); //Including␣LEMB-offset
I3ph[1]=_IQ12div(I3ph[1],␣_IQ12(17.2732)); //Scaling␣for␣5.273*1.3
I3ph[2]=Inverter::detail::st.curr[2]-_IQ12(0.15); //Including␣LEMC-offset
I3ph[2]=_IQ12div(I3ph[2],␣_IQ12(17.0352)); //Scaling␣for␣52*1.3


U3ph[0]=Inverter::detail::st.volt[0]+_IQ12(2.38); //Including␣the␣offset␣of␣LEMA-mea
U3ph[0]=_IQ12div(U3ph[0],_IQ12(12.585)); //11.308*0.58␣(pga␣scallering␣for␣spenning)
U3ph[1]=Inverter::detail::st.volt[1]+_IQ12(2.04); //Including␣the␣offset␣of␣LEMB-mea
U3ph[1]=_IQ12div(U3ph[1],_IQ12(12.738)); //11.438*0.58␣(pga␣scallering␣for␣spenning)
U3ph[2]=Uab_Uabc(U3ph[0],U3ph[1])+_IQ12(0.0); //Finding␣the␣Uca␣based␣in␣Uab␣and␣Ubc
U3ph[2]=_IQ12div(U3ph[2],_IQ12(1.0));

Udcbus=Inverter::detail::st.udc+_IQ12(4.2755); //DC-bus␣voltage␣measurements␣with
Udcbus=_IQ12div(Udcbus,␣_IQ12(215.00)); //scaling␣with␣regards␣to␣the␣LEM:␣1.723

Vdc=_IQ12toIQ(Udcbus); //Redefining␣the␣resolution␣of␣the␣parameters

//Finding␣the␣phase␣voltages␣for␣PLL
Uph[0]=Ull_Uph(U3ph[0],U3ph[2])
Uph[1]=Ull_Uph(U3ph[1],U3ph[0]);
Uph[2]=Ull_Uph(U3ph[2],U3ph[1]);


//Redefining␣the␣resolution␣of␣the␣parameters
```

```
i3[0]=_IQ12toIQ(I3ph[0]);
i3[1]=_IQ12toIQ(I3ph[1]);
i3[2]=_IQ12toIQ(I3ph[2]);

u3[0]=_IQ12toIQ(Uph[0]);
u3[1]=_IQ12toIQ(Uph[1]);
u3[2]=_IQ12toIQ(Uph[2]);

//Taking␣the␣clark␣transform␣of␣the␣current␣and␣voltages
smf28_iq20_clarke2(Ialfabeta,␣i3);
smf28_iq20_clarke2(Ualfabeta,␣u3);

//Calling␣the␣phase␣locked␣loop
thetaPll=phaseLockedLoop(Ualfabeta);

//Giving␣the␣angle␣value␣in␣pu.
thetaMod=_IQ20div(thetaPll,_IQ20(F_2PI));

//Performin␣the␣Park␣transform
smf28_iq20_rotate_pu(Idq,Ialfabeta␣,␣-thetaMod);
smf28_iq20_rotate_pu(Udq,Ualfabeta␣,␣-thetaMod);

//Filtering␣the␣input␣Park␣transformed␣variables

␣␣Idclass=thirdOrderButter(Idclass,␣Idq[0]);
␣␣␣␣Iqclass=thirdOrderButter(Iqclass,␣Idq[1]);
␣␣Udclass=thirdOrderButter(Udclass,␣Udq[0]);
␣␣␣␣Uqclass=thirdOrderButter(Uqclass,␣Udq[1]);
␣␣␣Udcclass=thirdOrderButter(Udcclass,␣Vdc);

//Calculating␣the␣reactive␣power␣from␣the␣converter
qGrid=reactiveCalculations(Udclass.y1,Iqclass.y1);

//DC-bus␣voltage␣controller
␣␣ireddc=pi_dcBus(Udcclass.y1);

␣␣//Reactive␣power␣controller
␣␣iredq=pi_ReacBus(Reacref,-qGrid);

//AC-current␣controllers␣->␣vector␣control
␣␣uOut[1]=pi_currentq(iredq,-Iqclass.y1,Idclass.y1,Uqclass.y1);
```

```
  uOut[0]=pi_currentd(-ireddc,Idclass.y1,Iqclass.y1,Udclass.y1);



//Inverse transforming the d,q->alfa/beta phasors
smf28_iq20_rotate_pu(UoutAlfabeta, uOut ,thetaMod);


//Controlling the magnitude of the output
my_mag=_IQ20abs(uOut[0]);

if(_IQ20abs(my_mag)>_IQ20(1.0))
{
my_mag=_IQ20(1.0);
}

//Finding the angle of the output vector
my_angle=_IQ20atan2PU(UoutAlfabeta[1],UoutAlfabeta[0]);

//Setting the PWM-signals
Inverter::ready_output_vector(my_mag, my_angle); //Built in function for setting the
```

C.2 Declared variables and functions

```
_iq20 my_mag; //input amplitude to the pwm-generator
_iq20 my_angle; //input angle to the pwm-generator
_iq20 thetaMod;
_iq12 I3ph[3]; //For measurements of currents
_iq12 Uph[3]; //For measurements of line voltages
_iq20 uab[2];
_iq12 Udcbus;
_iq20 ut[2];
_iq20 Vdc;
_iq20 i3[3];
_iq20 u3[3];
_iq20 qGrid;
_iq20 Reacref=_IQ20(0.0); //Reference reactive power. Inverted with regards to the c
_iq20 iredq;
```

```
//Class␣for␣the␣filtered␣measurements
testClass␣Udclass,Uqclass,Idclass,Iqclass,␣Udcclass;

////////////////////////////////////////////////////////////////////////

//The␣file␣contains␣the␣filter,␣PLL␣and␣control␣loops␣aplied
//
//////////////////////////////////////////////////////////////////////

////////////////////////////////////////////////////////////////////////

class␣testClass
{
public:
_iq20␣x1;
_iq20␣x2;
_iq20␣y1;
_iq20␣y2;
}␣test;


namespace␣filter
{
_iq20␣K1=_IQ20(0.9937);
_iq20␣K2=_IQ20(0.003132);
_iq20␣K3=_IQ20(0.003132);
}

_iq20␣fa,fb,fc;


//The␣filter␣applied␣to␣the␣park␣transformed␣currents␣and␣voltages
//NB!␣Not␣third␣order,␣but␣first␣order␣Butterworthfilter
testClass␣thirdOrderButter(class␣testClass␣intern,␣_iq20␣x_filter)
{

//Updating␣the␣input-␣and␣output␣variables
intern.y2=intern.y1;
intern.x2=intern.x1;
␣␣␣␣intern.x1=x_filter;
```

```
//Internal␣variables␣of␣the␣function:
fa=_IQ20mpy(filter::K1,intern.y2);
fb=_IQ20mpy(filter::K2,␣intern.x1);
fc=_IQ20mpy(filter::K3,␣intern.x2);

intern.y1=fa+fb+fc;

//returns␣the␣class␣with␣filtered␣values
return␣intern;

}


//Variables␣used␣in␣the␣interrupts␣file.␣Placed␣here␣for␣convinience
_iq20␣uOut[2]={0,0};
_iq20␣Ialfabeta[2]; //Contains␣the␣measured␣and␣transformed␣currents
_iq20␣Ualfabeta[2]; //Measured␣voltages,␣transformed␣by␣Clark-transform
_iq20␣Udq[2]; //Measured␣voltages,␣transformed␣by␣Park-transform
_iq20␣Idq[2]; //Measured␣currents,␣Park-transformed
_iq20␣UoutAlfabeta[2]; //The␣output␣space␣vector,␣before␣finding␣the␣pwm
_iq20␣thetaPll; //The␣estiamted␣voltage.


//Variables

namespace␣controllers
{
_iq20␣maks=_IQ20(1.0);

_iq20␣minst=_IQ20(0.0);

_iq20␣dcMax=_IQ20(1.0);

_iq20␣dcMin=_IQ20(0.0);

_iq20␣max2=_IQ20(1.0);

_iq20␣min2=_IQ20(-1.0);
}
```

```
namespace␣regVars //Contains␣the␣variables␣used␣in␣the␣control␣functions
{

//Declaration␣of␣the␣variables␣in␣current-q-controller
_iq20␣iqRef_int[2]; //Saves␣reference␣values␣of␣the␣current
_iq20␣iqMes_int[2]; //Saves␣the␣measured␣value␣of␣the␣current
_iq20␣i_eq[2]; //Voltage␣output␣of␣the␣regulator
_iq20␣i_uq[2];
_iq20␣uqOut;
_iq20␣uqDelt[2];

//Declaration␣of␣the␣variables␣in␣current-d-controller

_iq20␣idRef_int[2]; //Saves␣reference␣values␣of␣the␣current
_iq20␣idMes_int[2]; //Saves␣the␣measured␣value␣of␣the␣current
_iq20␣i_ed[2]; //Voltage␣output␣of␣the␣regulator
_iq20␣i_ud[2];
_iq20␣udOut;
_iq20␣udDelt[2];

//Declaration␣of␣the␣variables␣in␣the␣DC-controller

_iq20␣dcMes[2]={0,0};
_iq20␣dcOut[2]={0,0}; //Internal␣variable,␣used␣for␣limiting␣the␣output
_iq20␣edc[2]={0,0};

//Declaration␣of␣the␣variables␣in␣the␣Reactive␣power␣controller
_iq20␣ReacRef[2]={0,0};
_iq20␣ReacMes[2]={0,0};
_iq20␣ReacOut[2]={0,0}; //Internal␣variable,␣used␣for␣limiting␣the␣output
_iq20␣eReac[2]={0,0};

}


namespace␣current
{
_iq20␣K1=_IQ20(0.12938); //3.9088

_iq20␣K2=_IQ20(-0.1044); //3.7088
```

```
_iq20␣Ti_cross=_IQ20(0.0136);

_iq20␣K3=_IQ20(0.00124);

_iq20␣dLedd1,dLedd2,dLedd3;

_iq20␣qLedd1,qLedd2,qLedd3;

}

int␣i=0;
int␣j=0;


//Quadrature␣axis␣current␣control␣function
_iq20␣pi_currentq(_iq20␣iqref,␣_iq20␣iqmes,␣_iq20␣id_cross_mes,␣_iq20␣uq_ff_mes)
{

//Initalising␣the␣PI-output␣variables
if(i==0)
{
regVars::i_uq[0]=_IQ20(0);
regVars::i_uq[1]=_IQ20(0);
i=1;
}
//Rewriting␣the␣current␣vectors.␣Cell␣0␣contains␣always␣the␣newest␣value

regVars::iqRef_int[1]=regVars::iqRef_int[0]; //References
regVars::iqRef_int[0]=iqref;

regVars::uqDelt[1]=regVars::uqDelt[0];

regVars::iqMes_int[1]=regVars::iqMes_int[0]; //Measurements
regVars::iqMes_int[0]=iqmes;

regVars::i_eq[1]=regVars::i_eq[0]; //Updating␣the␣e[k-1]
regVars::i_uq[1]=regVars::i_uq[0]; //Updating␣the␣regulator␣output␣uq[k-1]

//The␣regulator␣equation:
```

```
regVars::i_eq[0]=(regVars::iqRef_int[0]-regVars::iqMes_int[0]); //calculating

current::qLedd1=-_IQ20mpy(current::K1,␣regVars::i_eq[0]); //e[k]␣term
current::qLedd2=-_IQ20mpy(current::K2,␣regVars::i_eq[1]); //e[k-1]␣term

current::qLedd3=_IQ20mpy(current::Ti_cross,id_cross_mes); //Cross␣coupling␣te

regVars::i_uq[0]=regVars::i_uq[1]+current::qLedd1+current::qLedd2;
regVars::uqOut=regVars::i_uq[0];
//Saturating␣the␣output␣with␣limitations␣to␣+/-␣1.0␣pu.
if(regVars::i_uq[0]<_IQ20(-0.5))
{
regVars::i_uq[0]=_IQ20(-0.5);
}
if(regVars::i_uq[0]>_IQ20(0.5))
{
regVars::i_uq[0]=_IQ20(0.5);
}

//Calculating␣the␣new␣output

regVars::uqDelt[0]=_IQ20mpy(current::K3,(regVars::i_uq[0]-regVars::uqOut));

regVars::uqOut=regVars::i_uq[0]+regVars::uqDelt[0]+regVars::uqDelt[1]+current

return␣regVars::uqOut;

}

//Direct␣axis␣current␣control␣function
_iq20␣pi_currentd(_iq20␣idref,␣_iq20␣idmes,␣_iq20␣iq_cross_mes,␣_iq20␣ud_ff_m
{
//Initalising␣the␣PI-output␣variables
if(j==0)
{
regVars::i_ud[0]=_IQ20(0);
regVars::i_ud[1]=_IQ20(0);
j=1;
}
//Rewriting␣the␣current␣vectors.␣Cell␣0␣contains␣always␣the␣newest␣value
```

```
regVars::idRef_int[1]=regVars::idRef_int[0]; //References
regVars::idRef_int[0]=idref;

//regVars::udDelt[1]=regVars::udDelt[0];

regVars::idMes_int[1]=regVars::idMes_int[0]; //Measurements
regVars::idMes_int[0]=idmes;

regVars::i_ed[1]=regVars::i_ed[0]; //Updating␣the␣e[k-1]
regVars::i_ud[1]=regVars::i_ud[0]; //Updating␣the␣regulator␣output␣uq[k-1]

//The␣regulator␣equation:

regVars::i_ed[0]=(regVars::idRef_int[0]-regVars::idMes_int[0]); //calculating␣e[k]

current::dLedd1=_IQ20mpy(current::K1,␣regVars::i_ed[0]); //e[k]␣term
current::dLedd2=_IQ20mpy(current::K2,␣regVars::i_ed[1]); //e[k-1]␣term

current::dLedd3=_IQ20mpy(current::Ti_cross,␣iq_cross_mes); //Cross␣coupling␣term

regVars::i_ud[0]=regVars::i_ud[1]+current::dLedd1+current::dLedd2;

//Saturating␣the␣output␣with␣limitations␣to␣+/-␣1.0␣pu.

regVars::udOut=regVars::i_ud[0];

if(regVars::i_ud[0]>controllers::maks)
{
regVars::i_ud[0]=controllers::maks;
}
if(regVars::i_ud[0]<controllers::minst)
{
regVars::i_ud[0]=controllers::minst;
}

regVars::udDelt[0]=_IQ20mpy(current::K3,(regVars::i_ud[0]-regVars::udOut));
regVars::udOut=regVars::i_ud[0]-current::dLedd3;␣//+ud_ff_mes;

return␣regVars::udOut;

}
```

```
////////////////////////////////////////////////////////////////////////////

_iq20 cdcLedd1, cdcLedd2;
_iq20 ireddc;

namespace dc
{
_iq20 K1=_IQ20(0.00253);

_iq20 K2=_IQ20(-0.002217);

}

//DC-bus voltage controller
_iq20 pi_dcBus(_iq20 dcmes)
{

_iq20 dcref=_IQ20(1.0);
//Rewrites the arrays, cell #0 contains always the newest value

regVars::dcMes[1]=regVars::dcMes[0];
regVars::dcMes[0]=dcmes;

regVars::dcOut[1]=regVars::dcOut[0];

regVars::edc[1]=regVars::edc[0];
regVars::edc[0]=dcref-regVars::dcMes[0];
//The regulator equation:
cdcLedd1=_IQ20mpy(dc::K1, regVars::edc[0]);
cdcLedd2=_IQ20mpy(dc::K2, regVars::edc[1]);
regVars::dcOut[0]=regVars::dcOut[1]+cdcLedd1+cdcLedd2;

//Limiting the output of the regulator
if(_IQ20abs(regVars::dcOut[0])>controllers::dcMax)
{
if(regVars::dcOut[0]<controllers::dcMin)
{
regVars::dcOut[0]=controllers::dcMin;
}
else
```

```
{
regVars::dcOut[0]=controllers::dcMax;
}

}
return␣regVars::dcOut[0];
}


////////////////////////////////////////////////////////////////////////////////

_iq20␣creacLedd1,␣creacLedd2,␣creacLedd3;


namespace␣qreg
{
_iq20␣K1=_IQ20(0.005385);

_iq20␣K2=_IQ20(-0.004615);

}


//Reactive␣power␣controller
_iq20␣pi_ReacBus(_iq20␣Reacref,_iq20␣Reacmes)
{

//Rewrites␣the␣arrays,␣cell␣#0␣contains␣always␣the␣newest␣value
regVars::ReacRef[1]=regVars::ReacRef[0];
regVars::ReacRef[0]=Reacref;

regVars::ReacMes[1]=regVars::ReacMes[0];
regVars::ReacMes[0]=Reacmes;

regVars::ReacOut[1]=regVars::ReacOut[0];
regVars::eReac[1]=regVars::eReac[0];

regVars::eReac[0]=regVars::ReacRef[0]-regVars::ReacMes[0];
//The␣regulator␣equation:

//The␣regulator␣equation:
```

```
creacLedd1=_IQ20mpy(qreg::K1,␣regVars::eReac[0]);
creacLedd2=_IQ20mpy(qreg::K2,␣regVars::eReac[1]);
regVars::ReacOut[0]=regVars::ReacOut[1]+creacLedd1+creacLedd2;

//Limiting␣the␣output␣of␣the␣regulator
if(_IQ20abs(regVars::ReacOut[0])>controllers::max2)
{
if(regVars::ReacOut[0]<controllers::min2)
{
regVars::ReacOut[0]=controllers::min2;
}
else
{
regVars::ReacOut[0]=controllers::max2;
}

}

return␣regVars::ReacOut[0];
}

_iq20␣reactiveCalculations(_iq20␣udinn,␣_iq20␣iqinn)
{
return␣_IQ20mpy(udinn,iqinn);
}

//Phase␣locked␣loop␣with␣variables

//Variables␣for␣the␣PLL:

_iq20␣eDiv;
_iq20␣fn[2]={0,0};
_iq20␣epll[2]={0,0};
_iq20␣fPrimpll[2]={0,0};

_iq20␣ipllab[2]={0,0};
_iq20␣iplldq[2]={0,0};

//The␣parts␣of␣the␣control␣equation
_iq20␣ledd1,␣ledd2,␣ledd3;
_iq20␣angle_pu;
```

```
//Definitions␣in␣pll
_iq20␣thetaP;
_iq20␣ledd5=_IQ20(0.000628);


namespace␣phaseLockLoop
{
_iq20␣K1=_IQ20(0.0000999); //Gain␣1␣pll

_iq20␣K2=_IQ20(1.5325); //Gain␣2␣pll

␣_iq20␣K3=_IQ20(1.5225); //Gain␣3␣pll

_iq20␣my2PI=_IQ20(F_2PI);
}

//End␣of␣variables␣for␣the␣PLL

//Variables␣for␣the␣park-transforms
_iq20␣voc[2]={0,0};
_iq20␣thetaIntern;


float␣dqSpennning[2];
testClass␣FilterDdclass,␣FilterQdclass;


//The␣phase␣locked␣loop

_iq20␣phaseLockedLoop(_iq20␣alfabetaComp[2])
{
_iq20␣fMax=_IQ20(40.0);
_iq20␣fSync=_IQ20(50.0);


thetaIntern=_IQ20div(voc[0],␣_IQ20(F_2PI));
smf28_iq20_rotate_pu(iplldq,␣alfabetaComp,␣-thetaIntern);

FilterDdclass=thirdOrderButter(FilterDdclass,␣iplldq[0]);
FilterQdclass=thirdOrderButter(FilterQdclass,␣iplldq[1]);
```

```
// ␣iplldq[0]=_IQ20mpy(alfabetaComp[0],_IQ20cos(voc[0]))+_IQ20mpy(alfabetaCom
// ␣iplldq[1]=_IQ20mpy(alfabetaComp[1],_IQ20cos(voc[0]))-_IQ20mpy(alfabetaCom

thetaP=_IQ20atan2(FilterQdclass.y1,␣FilterDdclass.y1);␣//finding␣the␣angle␣be
epll[1]=epll[0];
epll[0]=_IQ20(0)+thetaP;
fPrimpll[1]=fPrimpll[0];

//The␣PI-controller␣equation
ledd2=␣_IQ20mpy(phaseLockLoop::K2,epll[0]);

ledd3=␣_IQ20mpy(phaseLockLoop::K3,epll[1]);

ledd1=␣_IQ20mpy(fPrimpll[1],phaseLockLoop::K1);


fPrimpll[0]=ledd2+ledd3+ledd1;

//Limiting␣the
if(_IQ20abs(fPrimpll[0])>fMax)
{
if(fPrimpll[0]<-fMax)
{
fPrimpll[0]=-fMax;
}
else
{
fPrimpll[0]=fMax;
}
}
fn[1]=fn[0];
fn[0]=fPrimpll[0]+fSync;
voc[1]=voc[0];

voc[0]=_IQ20mpy(ledd5,(fn[0]+fn[1]))+voc[1];


if(voc[0]>phaseLockLoop::my2PI)
{
voc[0]=_IQ20(0);
voc[1]=_IQ20(0);
```

```
}
else
{
voc[0]=voc[0];
}

voc[1]=voc[0];
return␣voc[0];


}


//Symetrical␣load=>estimating␣the␣third␣voltage
_iq12␣U3ph[3];

_iq12␣Uab_Uabc(_iq12␣U1,_iq12␣U2)
{
return␣-(U1+U2);
}

//Line-phase␣voltage␣calculation
_iq12␣Ull_Uph(_iq12␣Ulla,␣_iq12␣Ullb)
{
return _IQ12mpy((Ulla-Ullb),_IQ12(0.577350));

}
```

D Additional laboratory results

D.1 Reactive power = -0.2 pu

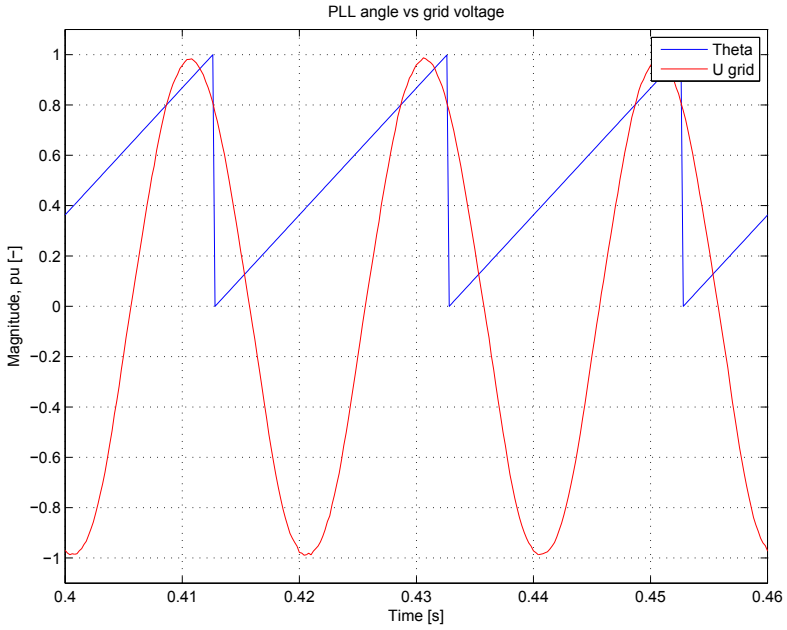

Figure D.1.1: PLL estimated angle and phase voltage

The PLL was expected to lock on the top of the phase voltage, fig. D.1.1, and hence, its response is of some concern. This is also the reason why the quadrature voltage of the PCC is unequal to zero. Hence, the PLL should be tuned better.

As a measure of the quality of the controllers, the deviations between the references and the controlled variables are given in fig. D.1.2. These are close to zero, and hence the quality of the controllers is acceptable.

The phase voltage is, as expected, sinusoidal. However, the shape of the current is showing that the switching is causing heavy distortion.

The angle of the converter is shifted from that of the phase locked loop, which is expected, as the quadrature axis of the converter is shifted to generate the demanded reactive power.

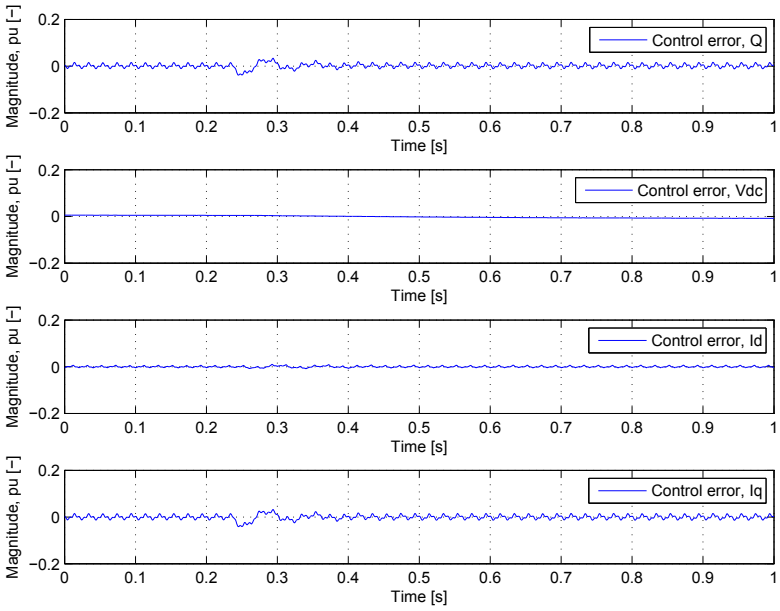

Figure D.1.2: Deviations in the controlled variables

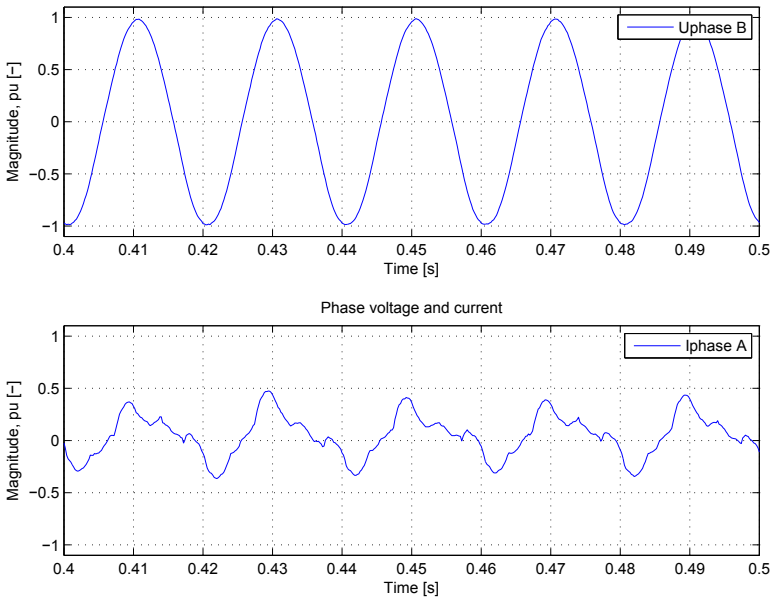

Figure D.1.3: Phase voltage and -current

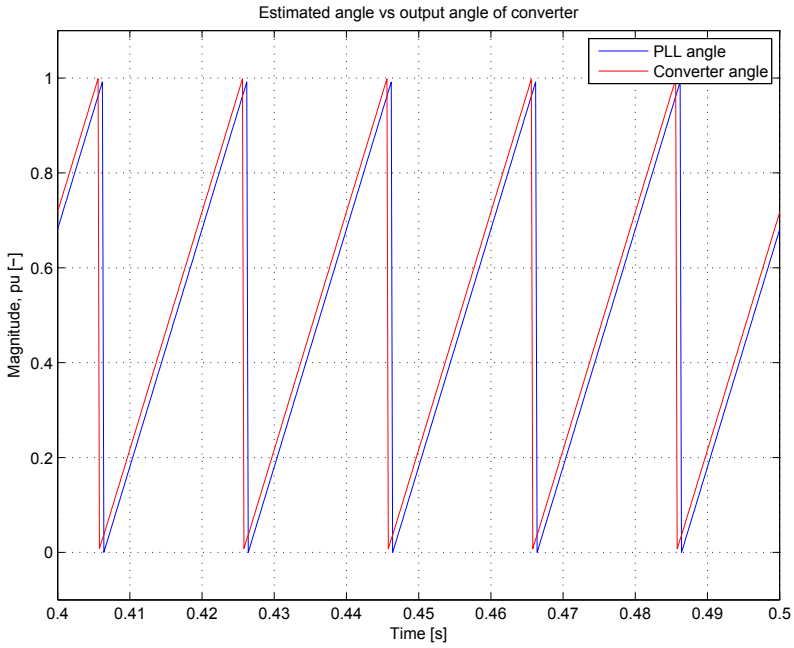

Figure D.1.4: PLL-angle and the angle of the converter output voltage

D.2 Reactive power = 0.2 pu

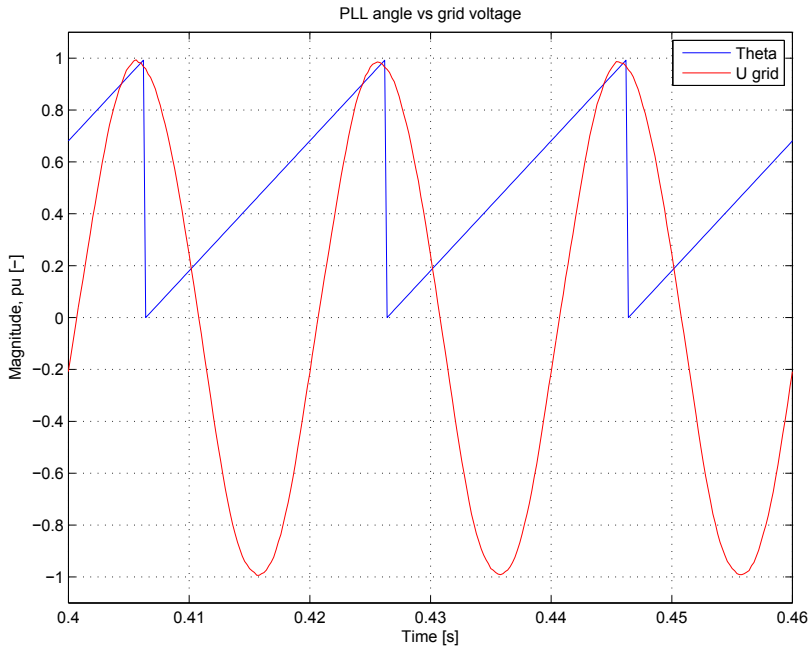

Figure D.2.1: PLL estimated angle and phase voltage

As mentioned above, the quality of the PLL could have been improved, and by this also improving the quality of the control system in general.

The deviations of the controllers are kept at a low, acceptable level.

The shape of the voltage is based on measurements taken at the PCC, and therefore, it is sinusoidal shaped. The current is controlled by the converter output, and is more disorted than the voltage.

The converter output angle, being shifted from the PLL, is in accordance with the expected, based on the values of $U_{q,conv}$.

The DC-bus controller is showing a satisfcatory behaviour, as it keeps the voltage steady.

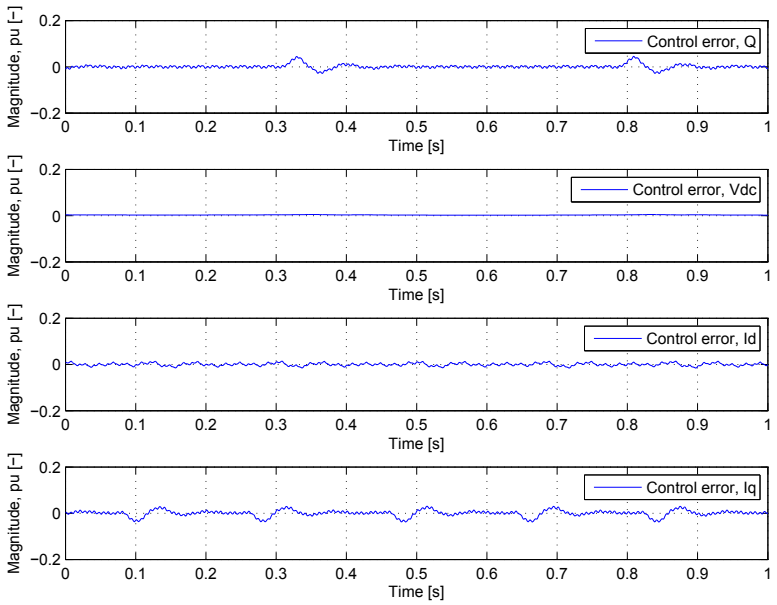

Figure D.2.2: Deviations in the controlled variables

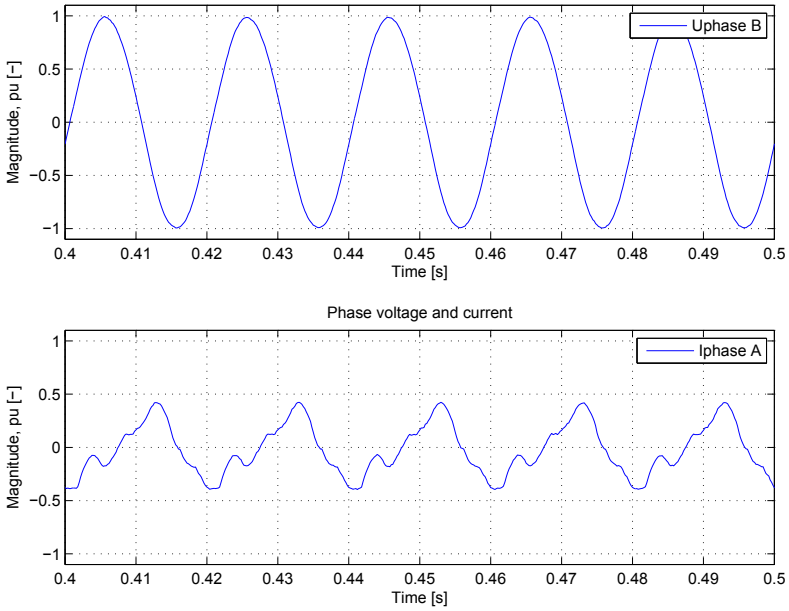

Figure D.2.3: Phase voltage and -current

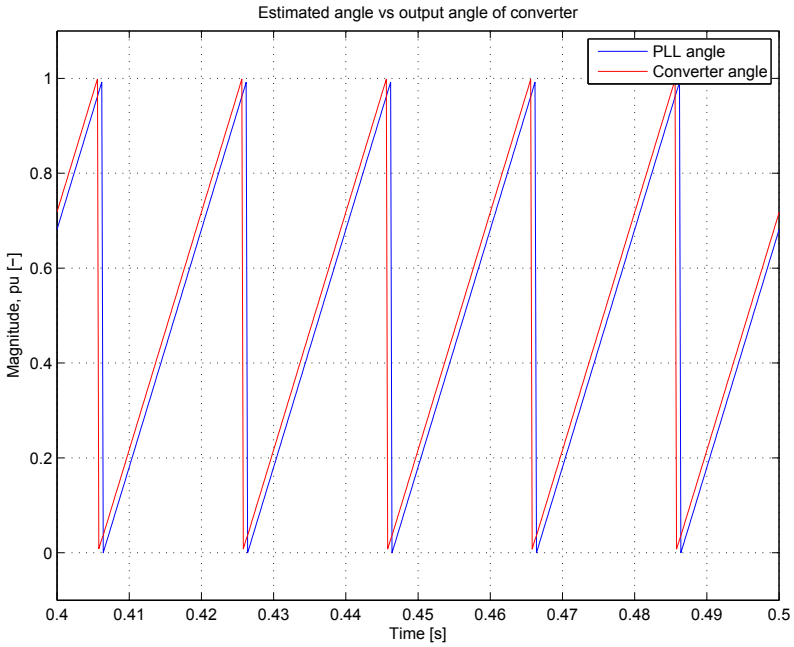

Figure D.2.4: PLL-angle and the angle of the converter output voltage

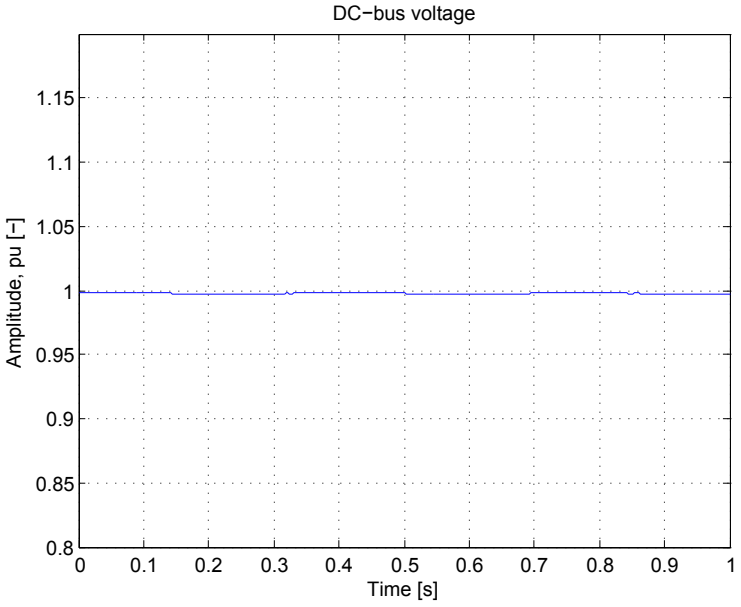

Figure D.2.5: DC-bus voltage

D.3 Reactive power = 0.0 pu

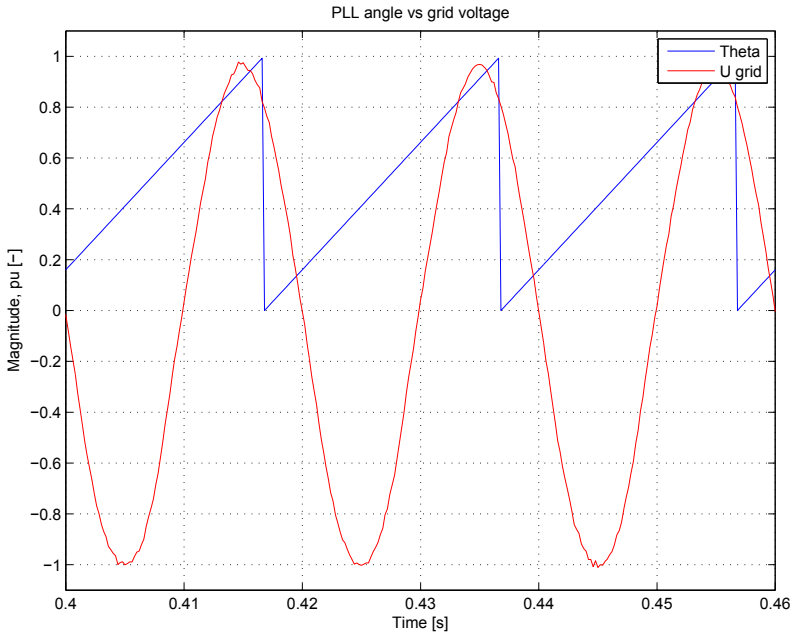

Figure D.3.1: PLL estimated angle and phase voltage

As in the abovementioned cases, the PLL is not locked on the top of the phase voltage.

For the controllers, the deviations are satisfacotry, and based upon the three cases presented here, it can be concluded that they are working like expected.

As in the above-mentioned cases, the current is disorted, while the grid voltage is having a satisfactory shape.

The PLL and the output vector angle is in phase, which is as expected when the reactive power output of the converter is set to zero.

The DC-bus voltage is kept steady, which indicates that the DC-bus voltage controller is working as expected.

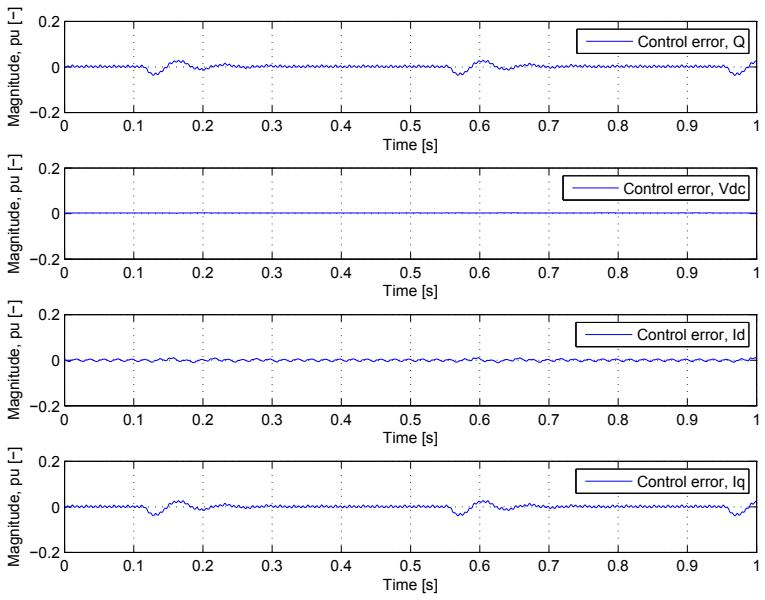

Figure D.3.2: Deviations in the controlled variables

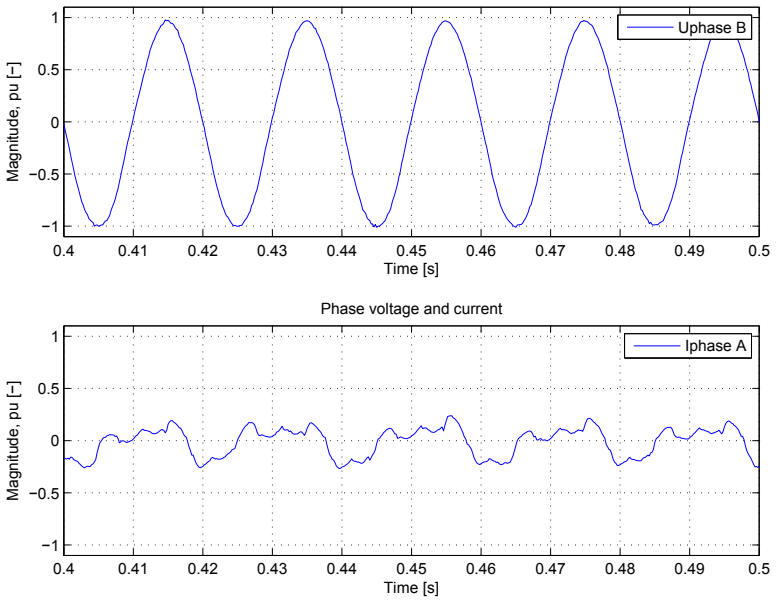

Figure D.3.3: Phase voltage and -current

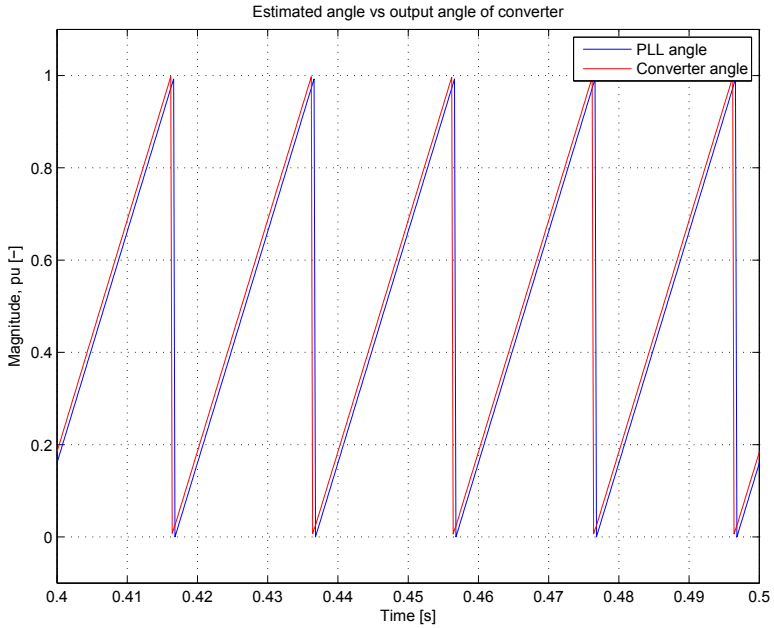

Figure D.3.4: PLL-angle and the angle of the converter output voltage

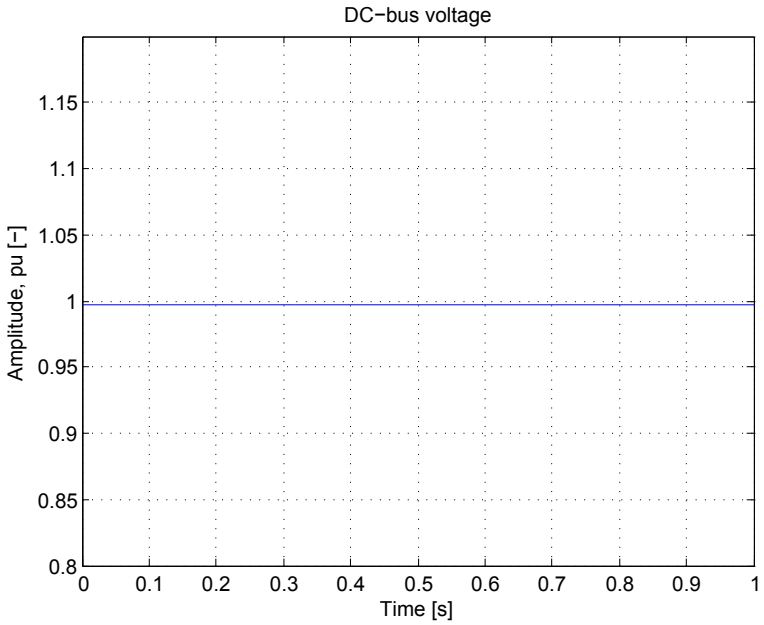

Figure D.3.5: DC-bus voltage

E Implementation of the PLL

The PLL used in the simulations was the one included in the library in PSCAD. However, the exact construction of this is not well documented, and therefore it proved difficult to produce a code for digital implementation. Therefore, the PLL used in [22], was implemented. The block scheme showing this is given below. The principle is based on taking the park transform of the voltages, and integrating up the devitation from the desired angle. The output of the control block is then added with the fundamental frequency, and integrated up in the voltage controlled oscillator. Then outcome of this is a ramp, which is reset to zero each time it reaches 2π. In the digital implementation of the PLL, the adding of $\pi/6$ is avoided by basing the park transform on the phase voltages instead of the line voltages.

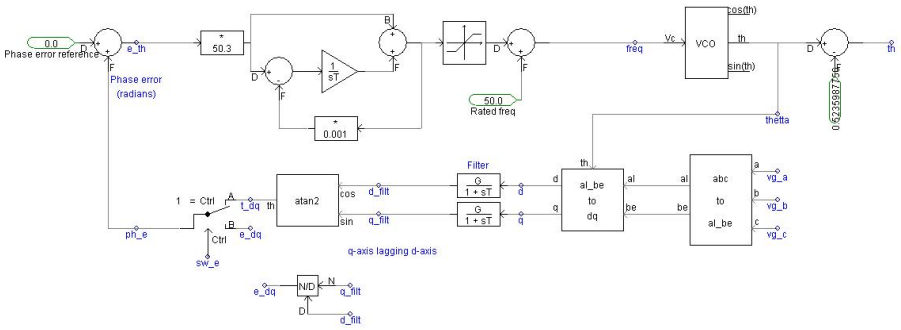

Figure E.0.6: The block scheme of the PLL implemented in the digital controller

F List of laboratory equipment

The following equipment was used during the work on experimental verification in the laboratory.

Type of instrument	*Detailed specification*
Oscilloscope	Tektronix TPS 2014
Variable AC transformer	Lübke VARIO 0-220V
Charging circuit	Custom built
Transformer	BI-357 5 kW 220V transformer
DSP	Texas Instruments TMS320C2800 F2812
Measuremnt card	NTNU/SEFAS 12x127.03, V1.0
Computer-DSP communication	RS-232 serial cable
Current measurement	LEM LA205-S
Voltage measurement	LEM LV25-P

Table F.0.1: Hardware laboratory equipment

Type	*Detailed specification*
Programming environment	Texas Instruments CodeComposerStudio v3.3
Operating environment	ActiveDSP v1.507
DSP-kernel	SmartMotor Kernel: SMF28 library

Table F.0.2: Software laboratory equipment

G Short discussion on the suitability of the SmartMotor kernel for students use

Learning and understanding to program a DSP fully out is a long and cumbersome process, which is, by some, claimed to take a couple of years. Even very spescialised implementation will take a long time when working on DSP for the first time. Texas Instruments provide some example files and peripheral files, which was used during the first steps of exploring the DSP during this work. However, putting these together to a well functioning control program would be a longlasting process, which could exceed the time of a master work. And therefore, the SmartMotor Kernel was taken into use. As mentioned in sec. 6.2.1, it provides the necessary platform for implementing the digital controller. In addition, SmartMotor are willing to consider providing more student lisences for the kernel for future master works.

The SmartMotor kernel program facilitates the work in the laboratory quite a lot, it leaves the user with an interface from which the implementation of digital control can be implemented. This means that a lot of heavy work on registers and peripherals is redundant, and a lot of time can be saved. However, to make a good working controller, a basic understanding of a DSP is necessary. At least, analog-digital converter (ADC), event manger (EV), interrupts and fixed point mathematics should be understood to some extent.

Also, because some parts of the program is hidden for the user ("black box"), a good contact with either SmartMotor, or an experienced user elsewhere is recommended, to avoid pitfalls while programming.

Regarding the limited time for a master thesis, and the fact that normally, not all time can be spent in the laboratory, the SmartMotor Kernel offers a good opportunity to realise digital control systems within the limits of a master work. Also, the student can, to some extent, choose how deep into the matter of DSP-programming he or she wishes to go, depending on the purpose of the laboratory implementation. Hence, further use of the SmartMotor kernel is recommended.